NACA TN 3170

NATIONAL ADVISORY COMMITTEE FOR AERONAUTICS

TECHNICAL NOTE 3170

AN EXPERIMENTAL INVESTIGATION AT LOW SPEEDS OF THE EFFECTS OF LIP SHAPE ON THE DRAG AND PRESSURE RECOVERY OF A NOSE INLET IN A BODY OF REVOLUTION

By James R. Blackaby and Earl C. Watson

Ames Aeronautical Laboratory
Moffett Field, Calif.

NACA

Washington
April 1954

NATIONAL ADVISORY COMMITTEE FOR AERONAUTICS

TECHNICAL NOTE 3170

AN EXPERIMENTAL INVESTIGATION AT LOW SPEEDS OF THE EFFECTS OF LIP SHAPE ON THE DRAG AND PRESSURE RECOVERY OF A NOSE INLET IN A BODY OF REVOLUTION

By James R. Blackaby and Earl C. Watson

SUMMARY

Wind-tunnel tests of a body of revolution with a circular nose inlet were conducted at low speeds to ascertain some of the effects of inlet lip bluntness and profile on diffuser performance and body drag. The tests were conducted at free-stream Mach numbers up to 0.330 with inlet flows from zero through choking. Both the angle of attack and the angle of yaw of the body were 0° throughout the investigation.

A sharp inlet lip profile was tested in addition to five circular-arc and two elliptical profiles; the various profiles were compared in terms of their shapes and contraction ratios, the ratio of the area circumscribed by the leading edge of the inlet lip to the minimum inlet area. As would be expected, the sharp lip provided the poorest pressure recovery for mass-flow ratios greater than 1.0 for all of the Mach numbers of the test. The improvement over the internal flow characteristics of the diffuser with the sharp lip, caused by a slight bluntness of the lip of the inlet, depended to only a small extent on the shape of the lip profile. However, for moderate bluntness the effect of the shape of the profile assumed importance, with an elliptical profile providing better pressure recovery than a circular profile.

Drag and surface-pressure measurements showed that for mass-flow ratios less than 1.0 the change of the external drag of the body with mass-flow ratio was caused almost entirely by the change of the suction pressures in the vicinity of the inlet. In addition, the magnitude of the change was found to be equal, but of opposite sign, to the change of the calculated additive drag for the inlet as long as the external flow was not separated from the lip.

Pressure and visual studies of the flow in the inlet indicated that a combination of oblique and normal shocks occurred in the inlet portion for mass flows near that required for choking. Pressure measurements in the diffuser indicated that, with the inlet choked, the amplitude of the total-pressure fluctuations was as great as 15 percent of the

free-stream total pressure. The frequency of these fluctuations was of the order of 20 cycles per second or less.

INTRODUCTION

Two factors to be considered in the selection of a lip profile for an inlet to supply air to a turbojet engine are the design Mach number and altitude and off-design operation. Generally speaking, the first of these factors is of primary importance and for good performance a sharp lip profile is required for supersonic flow and a rounded lip profile is required for subsonic flow. The second factor may assume importance with a sharp lip inlet during subsonic operation (e.g., take-off, landing, or cruising), and some compromise of the design may be necessary to insure satisfactory over-all performance.

One of the purposes of the present investigation was to study some of the effects of lip bluntness and profile on the characteristics of an inlet at zero and low subsonic speeds and for inlet mass flows from zero through choking. A body of revolution with a removable, circular nose-inlet portion was selected for the investigation. The lip profiles tested included a sharp lip, five lips with circular-arc profiles providing contraction ratios (the ratio of the area encompassed by the leading edge of the inlet to the minimum inlet area) of approximately 1.04, 1.08, 1.16, 1.24, and 1.33, and two lips with elliptical profiles providing contraction ratios of approximately 1.08 and 1.18.

In the case of ideal potential flow about a lip of finite thickness, two-dimensional theory (ref. 1) indicates that the lip suction force for mass-flow ratios less than 1.0 is exactly equal to the calculated additive drag of the entering flow (refs. 2 and 3). An additional phase of the present investigation was the measurement of body drag and of the pressures on the external surface of the body with different lips in order to make a comparison of the increments of body drag, lip suction force, and calculated additive drag resulting from a change of mass-flow ratio (for mass-flow ratios below 1.0).

The investigation was conducted in one of the Ames 7- by 10-foot wind tunnels for a range of free-stream Mach numbers up to 0.330. Both the angle of attack and angle of yaw were 0°.

NOTATION

The following symbols and subscripts are used in this report:

A area, sq ft

A_F maximum frontal area of test body, 0.785 sq ft

a	amplitude of total-pressure fluctuations, lb/sq ft
C_D	drag coefficient, $\frac{D}{q_o A_F}$
D	drag, lb
D_a	additive drag, lb
D_T	total drag measured by the strain gage, minus the seal tare force, lb
f	frequency of total-pressure fluctuations, cps
H	total pressure, lb/sq ft
h	radial distance in from wall of inlet, in.
M	Mach number
M_1	average inlet Mach number, calculated assuming entire measured total-pressure loss (H_o-H_3) to occur ahead of station 1
M_1'	average inlet Mach number, calculated assuming entire total-pressure loss (H_o-H_3) to occur after station 1
m	mass-flow rate (ρAV), slugs/sec
m_o	reference mass-flow rate ($\rho_o A_1 V_o$), slugs/sec
m^*	mass flow required to choke inlet, assuming isentropic flow from free stream to station 1, slugs/sec
P	static-pressure coefficient, $\frac{p-p_o}{q_o}$
p	static pressure, lb/sq ft
q	dynamic pressure, lb/sq ft
r	radius, in.
V	air velocity, ft/sec
x	axial distance, in.
y	ordinate measured normal to body axis, in.
γ	ratio of specific heats for air, 1.4
ρ	mass density of air, slugs/cu ft

Subscripts

e	conditions at the inlet to the 5-inch-diameter sting (exit of the ducted portion of the sting-mounted body), station 79.50
ext	drag components acting on the external surface of the sting-mounted body and on the outside of the stagnation streamline of the flow entering the inlet
i	drag components acting on the inner surface of the sting-mounted body and on the inside of the stagnation streamline of the flow entering the inlet
l	local conditions in the internal flow
max	maximum-frontal-area station of the body, station 72.0
s	conditions at the stagnation station on the inlet lip
t	conditions at the trailing edge of the sting-mounted body, station 117.0
o	conditions in the free stream
1	average conditions at the exit of the constant-area portion of the inlet, station 15 (A_1 = 0.0942 sq ft)
3	average conditions at a simulated engine-compressor entrance station, station 36.25 (A_3 = 0.1389 sq ft)

MODEL DETAILS

The model used in the tests was a streamline body of revolution with internal ducting and provisions for mounting interchangeable inlet portions at the nose (figs. 1 and 2). The maximum diameter of the body was 12 inches at station 72.00. Two afterbodies were used. The first (figs. 1 and 3(a)) was mounted on an 8-inch-diameter vertical strut through which the inlet air flow could be exhausted from the body. With this afterbody, the total body length was 129 inches. The second afterbody was mounted on a 5-inch-diameter horizontal sting (figs. 1 and 3(b)) through which air could be drawn. The body was mounted on the sting by the use of flexure-pivot assemblies, as shown in detail B, figure 1, which resisted torsional, pitching, and lateral loads but permitted axial movement. The axial movement was restrained by a strain gage used to measure the axial forces on the body (detail A, fig. 1). Leakage of air between the sting and the afterbody was prevented by a rubber

dental-dam seal, shown in detail B, figure 1. With this afterbody, the total body length was 117 inches.

The interchangeable inlet portions (fig. 2) were machined from aluminum or brass castings, and all the lip profiles tested were formed within the boundaries of a basic sharp-edged inlet. This sharp-edged inlet was formed with a conical outer surface tangent to the basic forebody at station 14.118 and with a cylindrical inner surface with a radius of 2.078 inches, extending from the sharp leading edge, station 9.00, to station 15.00. The angle between the inner and outer surfaces was about 7-1/2°. A bell mouth was designed for installation with this sharp-edged inlet.

In addition to the sharp-edged inlet, two other types of profiles were employed in the tests. One was a circular-arc type and the other was made up of an elliptical inner profile and an approximately elliptical external profile. (The two types of profiles will be referred to as circular type and elliptical type in the rest of the report.) Both types of profiles were tangent to the surfaces forming the sharp-edged inlet. The ratio of the minor axis to the major axis of the ellipse forming the internal shape of the elliptical-type profiles was 0.2777.

Five circular- and two elliptical-type profiles were tested. They are identified by lip-designation numbers and letters as shown in figure 2. The number is an index of the bluntness of the lip and is equal to the decimal portion of the inlet contraction ratio to the nearest hundredth. The letter R indicates a circular profile, and the letter E, an elliptical profile. Thus, lip 24R had a circular-arc profile and the area encompassed by the leading edge of the resulting inlet was approximately 24 percent (actually 24.3 percent, as tabulated in fig. 2) greater than the minimum inlet area. The minimum inlet area was equal to 12 percent of the maximum frontal area of the body.

The diffusion ratio of the internal duct (defined as the ratio of the flow area at the simulated compressor entrance station—station 36.25 - to the minimum inlet area) was 1.474. The included angle of the unobstructed conical portion of the diffuser - from station 15.00 to station 32.00 - was about 4°.

INSTRUMENTATION AND TESTS

For both model-support arrangements, the flow of air through the inlet and subsequent ducting was regulated by an exhaust pump outside the wind-tunnel test chamber. The rate of inlet air flow was measured by a calibrated orifice meter. Tests were conducted at free-stream Mach numbers of 0, 0.115, 0.166, 0.237, and 0.330 with Reynolds numbers of about 0, 68,000, 96,000, 136,000, and 185,000 per inch, respectively. The range of inlet-air-flow rates during the tests was from zero through

choking, and the angle of attack and angle of yaw of the body were 0°. Boundary-layer transition on the body was fixed by a 1/2-inch-wide band of carborundum grains at station 15.00 for the entire investigation. No tunnel-wall corrections were applied to any of the data.

Strut-Supported Model

With the model mounted on the 8-inch-diameter strut, the loss of total pressure from the free stream to the simulated turbojet-engine compressor inlet, station 3 (station 36.25 in., fig. 1), was measured by a rake consisting of 24 total-pressure and 4 static-pressure tubes. The total-pressure loss was measured for mass-flow ratios m_1/m_0 from zero through choking for each lip and each test Mach number.

Studies of the total- and static-pressure variations at several stations in the minimum-area section of the inlet with lips 0 and 16R were made using a small two-tube rake extending through the wall of the inlet. The distance from the rake tubes to the internal wall of the duct was adjustable from outside the wind-tunnel test section.

With no external air flow (i.e., static conditions), the variation of the static pressure down the center line of the inlet with lips 0 and 16R was measured for various inlet mass flows. For these tests a long static-pressure probe was utilized which extended into the inlet from the quiet-air region well ahead of the inlet.

For these same two lips, visual studies of the flow into the inlet for $M_0 = 0$ were made using the splitter-plate setup shown in figure 4. This plate extended the length of the constant-area section of the duct and fitted tightly both inside and outside the inlet. For each of several inlet mass flows, a mixture of kerosene and lampblack was sprayed onto the plates and into the air stream approaching the inlet. The resulting flow patterns on the plates were photographed.

For lips 0 and 16R, the fluctuations of total pressure in the diffuser section of the duct ahead of station 3 were measured utilizing a 3/8-inch-diameter sensitive total-pressure probe (which housed a diaphragm and strain gage) and were recorded by an oscillograph. These measurements were made for various inlet mass flows with free-stream Mach numbers of 0, 0.237, and 0.330.

Sting-Supported Model

Drag measurements were made with the model mounted on the 5-inch-diameter sting for free-stream Mach numbers of 0.237 and 0.330 and

mass-flow ratios up to 1.0 with lips 0, 16R, and 18E. In addition, the drag of the basic pointed-nose body was measured for the same Mach numbers.

The total drag of the model was measured by a calibrated strain gage which resisted the axial movement permitted by the flexure-pivot mounting system. The strain gage was mounted between the afterbody and the sting as shown in detail A, figure 1. The total internal drag, based on the total-momentum loss from the free stream to the entrance to the sting, was calculated from measurements of the pressures at station e, the sting entrance. These pressures were measured with a rake consisting of 37 total-pressure and 4 static-pressure tubes.

The rubber dental-dam seal shown in detail B, figure 1, caused a small axial load on the body. The variation of this load was calibrated against the pressure difference across the seal, measured by two static-pressure orifices connected to a manometer. The load imposed by the seal as indicated by the pressures across the seal during the tests was thus subtracted as a tare force from the strain-gage drag measurements.

The surface-pressure distribution along the body was measured for the sting-mounted model with lips 0 and 16R for various mass-flow ratios and a free-stream Mach number of 0.237. One row of static-pressure orifices was provided along the inlet portion and the body at the stations tabulated in figures 1 and 2.

RESULTS AND DISCUSSION

Internal-Flow Studies With the Strut-Mounted Model

Total-pressure recovery and mass-flow ratio.- The variations of total-pressure recovery H_3/H_0 measured at the simulated compressor entrance and of the mass-flow ratio m_1/m_0 with compressor-entrance Mach number M_3 for the inlet with each of the lips are shown in figures 5(a) to 5(d) for free-stream Mach numbers from 0.115 to 0.330. Data were obtained for mass-flow ratios from zero through choking for each lip. For a free-stream Mach number of zero, the variations of the total-pressure recovery and of the mass-flow ratio m_1/m^* with compressor-entrance Mach number are shown in figure 6. The mass-flow ratio m_1/m^* is based on the weight rate of air flow required to choke the inlet with isentropic flow assumed from free stream to the inlet. Also shown in figure 6 are the variations of H_3/H_0 and m_1/m^* with M_3 for the model with a bell mouth at the inlet. A curve of the variation of mass-flow ratio computed for the case of isentropic flow from free stream to the compressor entrance is included in figures 5 and 6.

In figures 7(a) to 7(h) the data of figure 5 have been cross-plotted to form composite curves of the variation of total-pressure recovery with free-stream Mach number for constant mass-flow ratios.

Using the data in figure 5, curves of constant compressor-entrance Mach number M_3 (such as $M_3 = 0.44$) may be included on the composite curves of figure 7. Similarly, curves of constant inlet Mach number (M_1 = constant) may be superimposed by utilizing the curve in figure 8 which was calculated using the following equation with the assumption of isentropic flow from station 1 to station 3 ($H_3 = H_1$):

$$\frac{M_1}{\left(1 + \frac{\gamma-1}{2} M_1^2\right)^3} = \frac{H_3}{H_1}\frac{A_3}{A_1}\left[\frac{M_3}{\left(1 + \frac{\gamma-1}{2} M_3^2\right)^3}\right] \qquad (1)$$

For the model used, the diffusion ratio A_3/A_1 was 1.474. It can be seen (fig. 8) that with the assumption of isentropic diffuser flow, the $M_3 = 0.44$ curve in figure 7 would correspond with the curve for $M_1 = 1.00$. A third family of curves which could be superimposed on those in figure 7 would be curves of constant inlet Mach number M_1', calculated on the basis of the measured weight rate of air flow and the minimum inlet area (0.0942 sq ft) and with the total-pressure recovery H_1/H_0 assumed to be 1.00. Inlet Mach number, defined in this manner, has been used frequently in performance analyses of air-induction systems and is, therefore, presented in figure 9 for the free-stream Mach numbers of the present investigation as a function of mass-flow ratio m_1/m_0.

Study of figures 5, 6, and 7 shows that, as would be expected, the total-pressure recovery and mass-flow characteristics of inlets with circular-profile lips improve with increasing bluntness. The characteristics of the bluntest profile tested, lip 33R, approached the isentropic and bell-mouth characteristics even for a free-stream Mach number of zero. The characteristics of lip 8E were comparable with those of blunter circular lips for mass-flow ratios up to about 1.5. For higher mass-flow ratios, however, the total-pressure recovery was nearly the same as for lip 8R. The characteristics of lip 18E are comparable with those of lip 33R for free-stream Mach numbers other than zero for most of the mass-flow range. For a free-stream Mach number of zero (fig. 6), its characteristics were still better than would be measured for a circular profile of the same contraction ratio. (Note that contraction ratio and bluntness are used synonymously in comparing the lip profiles.)

The higher total-pressure recoveries possible with the elliptical profiles are thought to result because separation from the internal lip surfaces was delayed to higher mass-flow ratios than with circular profiles of similar bluntness. When separation did occur from an elliptical profile, it appears that its characteristics immediately became comparable to those of a circular profile with an equal contraction ratio.

In view of the fact that the bell-mouth data indicate small diffuser losses, the lip data presented should be reasonably applicable to any well-designed diffuser of moderate diffusion ratio. To facilitate such use of the data, the conversion curves in figure 10, calculated by use

of equation (1), are presented. By entering the curves with any M_3 of the present investigation (plotted as abscissa) and by going to the desired diffusion ratio A_3/A_1, the corresponding M_3 for the desired diffuser may be read as the ordinate.

Inlet choking conditions.- The approximate compressor-entrance Mach number for which choking first occurred in the inlet with each of the lips may be found in figures 5 and 6 as the M_3 above which there was no apparent increase in mass-flow ratio. The choking M_3 thus defined may be seen to have been near 0.44 in most cases (computed from the measured weight rate of air flow and total-pressure ratio). Deviations from this value, down to about 0.40 for lip 0, and up to about 0.455 for the bell mouth (both conditions estimated for a free-stream Mach number of zero from fig. 6) can be seen. For the case of the bell mouth it was assumed that choking corresponded with the attainment of an average Mach number of 1.0 in the inlet ($M_1 = 1.0$); a diffuser total-pressure ratio H_3/H_1 of 0.98 was then calculated using equation (1). (If this total-pressure ratio, 0.98, applies at choking regardless of the lip shape or free-stream Mach number, the majority of the total-pressure losses measured at the compressor-entrance station must have occurred at the lip or in the constant-area inlet portion of the duct.)

With the assumption of a constant diffuser total-pressure ratio of 0.98, any reduction of M_3 from 0.455 can be shown by equation (1) to correspond with a reduction of inlet Mach number from 1.0. In the case of lip 0, for static free-stream conditions an inlet Mach number of 0.69 corresponds to the choking M_3 of 0.40 and, from figure 6, the choking values of m_1/m^* and H_1/H_0 can be found to be about 0.75 and 0.832 (i.e., 0.816/0.98), respectively. These values of choking mass-flow ratio and the total-pressure ratio are in contrast to the theoretical choking values calculated in reference 4:

$$\frac{m_1}{m^*} = \frac{H_1}{H_0} = 0.79$$

The lower choking mass-flow ratio measured in the present investigation, 0.75, is thought to be an indication of the extent to which the actual inlet-flow phenomena differ from those associated with the theory. The inequality of the experimental choking mass-flow ratio and inlet total-pressure ratio arises because the corresponding average inlet Mach number was, as shown above, less than 1.0. The continuity equation as used in reference 4 may be written

$$\frac{m_1}{m^*} = 1.728 \frac{H_1}{H_0} \frac{M_1}{(1 + 0.2 M_1^2)^3}$$

and it can be seen that

$$\frac{m_1}{m^*} = \frac{H_1}{H_0}$$

only when $M_1 = 1.0$. These equations should be applicable regardless of lip shape. From equation (1) with $H_3/H_1 = 0.98$ and an assumed inlet Mach number of 1.0, M_3 would be 0.455 (as indicated by the data of fig. 6 for the bell mouth), and the corresponding inlet total-pressure ratio H_1/H_0 would be nearly equal to the choking mass-flow ratio m_1/m^*. The compressor-entrance Mach number, $M_3 = 0.44$, corresponding to isentropic expansion from uniform sonic flow at the inlet entrance, is included on the composite curves of figure 7. In addition, the approximate experimental choking limits are shown.

Total-pressure fluctuations in the diffuser.- Oscillograph records for the flow, a few inches ahead of station 3, were interpreted as shown in the following idealized sketch of a typical record for conditions near choking:

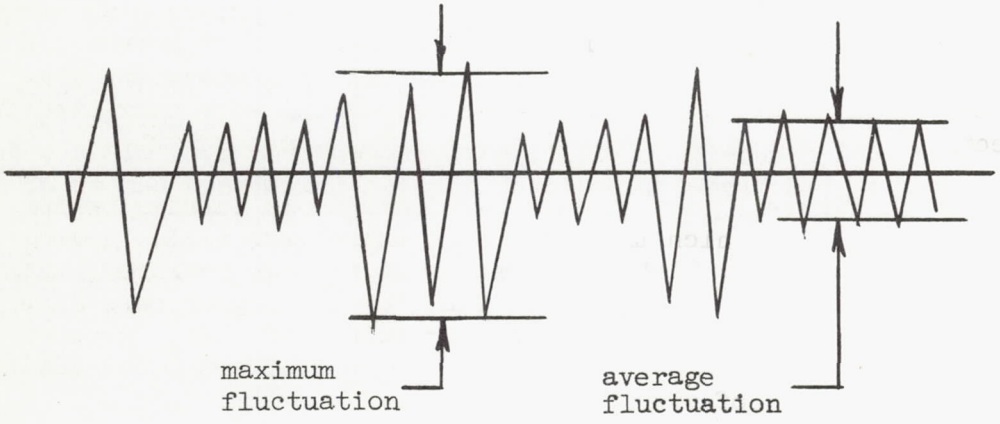

Two types of pressure fluctuations are seen to have occurred simultaneously. The first type, termed the "average fluctuation," was determined ignoring the occasional large-amplitude, low-frequency fluctuations, termed the "maximum fluctuation," which made up the second type. The frequency and amplitude of both the average and the maximum fluctuations are shown in figures 11(a) and 11(b) for the model with lips 0 and 16R, respectively, and for free-stream Mach numbers of 0, 0.237, and 0.330. The intensity of the fluctuations is expressed as the total amplitude divided by the free-stream total pressure. The major part of the data were recorded for mass flows near choking, and the random, aperiodic nature of the fluctuations made the interpretation of the oscillograph records difficult.

The static characteristics of the sensitive pressure cell and oscillograph equipment (amplitude ratio a/H_o of about 0.02 with a frequency of 60 cycles per second) are indicated in figures 11(a) and 11(b) by a dash at zero compressor-entrance Mach number. Complete interpretation of the variations of frequency and amplitude is not attempted; however, the curves are consistent in indicating the occurrence of large-amplitude low-frequency pressure fluctuations which may be of importance for mass flows near choking for the inlet with either of the two lips. The amplitudes of the fluctuations were as much as 15 percent of the free-stream total pressure with a frequency of less than 20 cycles per second when the inlet was choked. No attempt was made to calculate the extent to which these effects may be attributable to the resonant characteristics of the duct tested.

Pressure studies in the inlet portions.- The results of static- and total-pressure surveys at several axial stations in the inlet portion for lips 0 and 16R for a free-stream Mach number of zero are presented in figures 12(a) and 12(b). For lip 0, surveys are included for two mass flows below choking (M_3 = 0.30 and 0.36), while for lip 16R, surveys are included for one mass flow below choking (M_3 = 0.38), and for the choked condition with M_3 = 0.46. The corresponding variations of local Mach number, calculated using tables of M versus p/H (ref. 5) are also included in figure 12. For the regions where the local flow was supersonic, the local total pressures were corrected for the effects of the shock wave ahead of the total-pressure tube.

For lip 0, figure 12(a), the surveys indicate an annular region near the inlet wall in which the local Mach number was zero. Immediately inside this region, high local Mach numbers were measured, with a maximum local Mach number in excess of 1.20 for the higher mass flow. The reductions of total-pressure ratios for values of h/r_1 greater than 0.2 at the two rear survey stations (x/r_1 = 0.40 and 0.84) indicate the possible existence of shocks in the flow.

For lip 16R, examination of the curves in figure 12(b) indicates that the annular region of $M_1 = 0$ was, of course, much smaller than that for lip 0. The maximum local Mach number attained was about 1.45 near the wall at the forward survey station (x/r_1 = 0.27). At the second survey station (x/r_1 = 0.72), this high Mach number flow had been replaced, probably as a result of local shock waves, by a region of fairly steady flow having a Mach number between 0.9 and 1.0.

In figure 13, inlet pressure-survey data for lips 0 and 16R are presented for a mass-flow ratio of about 1.5 for three free-stream Mach numbers. An annulus of low-speed flow is seen to have existed near the inlet wall for both lips, although its extent was less than that for the static tests (fig. 12). Away from the inlet wall, the local Mach number was fairly constant for both lips, with higher local Mach numbers being measured with lip 0 than with lip 16R. Data are presented for only one survey station for each lip because similar total-pressure profiles

were measured at the other survey stations. Similarly, the measurements are presented for only one mass-flow ratio because the effect of variation of mass-flow ratio (below choking) was found to be manifested as a change in the magnitude of the local Mach number away from the inlet wall.

The static-pressure variation down the center line of the inlet portion with lips 0 and 16R with a free-stream Mach number of zero is presented in figures 14(a) and 14(b). Flow conditions approximating those for which the data in figures 12(a) and 12(b) are presented were maintained for these static-pressure measurements. If it is assumed that there was no total-pressure loss in the flow at the center of the inlet, the flow would be subsonic until p_l/H_0 was reduced to 0.528. This value is indicated in figure 14. The local static pressures measured during the choked operation of the inlet with lip 16R (fig. 14(b)) indicate that a maximum local Mach number near 1.4 was attained at the center line at x/r_1 of about 1.1. The abrupt rise in static pressure immediately downstream of this station is thought to have occurred in an oblique shock since the pressure rise was not great enough to signify the presence of a normal shock with subsequent subsonic flow. The flow following the pressure rise (downstream from $x/r_1 = 1.4$) is considered to have remained supersonic until the second abrupt static-pressure rise (downstream of $x/r_1 = 2.2$) when a normal shock is thought to have occurred. The location of this disturbance was not determined exactly but seemed to vary between $x/r_1 = 2.3$ and $x/r_1 = 2.6$.

Visual flow studies in the inlet portions.- In connection with the pressure studies of the flow in the inlet section with lips 0 and 16R, visual studies of the flow were made for a free-stream Mach number of zero utilizing kerosene and lampblack as described in the section Instrumentation and Tests. The flow phenomena noted are indicated schematically for lip 0 in figure 15. Pictures of the flow formed on the splitter plates by the kerosene and lampblack mixture are shown in figures 16 and 17. Inasmuch as the flow lines were influenced by the boundary layer on the plates and by the mass and viscosity of the kerosene and lampblack mixture, they must be regarded as only qualitative indications of the inlet flow.

The cause of the discontinuity of the flow lines, corresponding with line A, figure 15, which was present for the inlet with either lip for all mass flows is not understood. The boundary indicated by line B, figure 15, appears to define the region of separated flow near the inlet lips and the growth of the boundary layer along the inlet wall after reattachment of the flow. It can be seen that for the lower mass flows, the area thus defined as the boundary layer grew quite rapidly for both lips 0 and 16R, but that, as the mass flow was increased to the choking range (M_3 greater than 0.4), the thickness of the layer decreased, especially with lip 16R.

The discontinuity designated by line C in figure 15 is thought to be an indication of an oblique shock wave which originated in the region where the separated flow from the lips returned to the inlet wall. Line N, in figure 15, is thought to be the indication of a normal shock in the flow. The vortices, line V, indicate a flow phenomenon in the boundary layer on the plate behind the normal shock. The locations of the shocks, as shown by the pictures, are in general agreement with the interpretation of the data of figure 14.

In conjunction with the studies of the inlet flow reported thus far, visual observations of the cloud of condensed water vapor in the low-pressure regions in the inlet were made with both lips 0 and 16R throughout the mass-flow range for a free-stream Mach number of zero. As the mass-flow rate was increased to values near choking for lip 0, condensation first appeared in an annulus near the inlet walls. With increasing mass flow, the area of condensation extended inward until it was visible over essentially the entire inlet area for the mass flow at which the inlet was choked. In the choked condition, the central region of the condensation cloud appeared extremely unsteady as evidenced by a fore-and-aft oscillation. During the operation of lip 16R, the progression of condensation from the annulus to the complete filling of the inlet occurred over a smaller range of mass flows.

Drag and Surface-Pressure Studies With the Sting-Supported Model

Drag measurement.- The total drag of the model is defined as the load measured by the strain gage minus the seal tare and is designated D_T. The internal drag is calculated in the conventional manner based on the change of total momentum of the internal air flow from free stream to the exit from the ducted portion of the body (station e, fig. 1)

$$D_{i,o-e} = m(V_o-V_e) - A_e\ (p_e-p_o) \tag{2}$$

The internal drag thus defined is made up of two parts

$$D_{i,o-e} = D_{i,o-s} + D_{i,s-e} \tag{3}$$

In this equation, the portion of the internal drag ahead of the inlet may be defined as

$$D_{i,o-s} = m(V_o-V_s) - A_s\ (p_s-p_o) \tag{4}$$

The additive drag for an inlet (refs. 2 and 3) is defined as

$$D_a = D_{ext,o-s} = \int_{surface} (p-p_o)\ dA \tag{5}$$

It can also be shown that

$$D_a = m(V_s - V_o) + (p_s - p_o) A_s \tag{6}$$

Comparing equations (4) and (6)

$$D_{i,o-s} = -D_a \tag{7}$$

Equation (7), in conjunction with equation (3), is of significance in that it shows additive drag to be a hypothetical force which enters into consideration because of the definition of internal drag in equation (3).

The total external drag of the model, defined in the same manner as internal drag, is expressed as

$$D_{ext,o-t} = D_a + D_{ext,s-t} \tag{8}$$

and in terms of total drag

$$D_{ext,o-t} = D_T - D_{i,o-e} \tag{9}$$

The drag component $D_{ext,s-t}$ in equation (8) will be referred to in the remainder of the report as the external body drag.

A sample plot of data is included as figure 18. The experimental values of C_{D_T} and $C_{D_{i,o-e}}$ are shown as functions of mass-flow ratio for lip 18E for a free-stream Mach number of 0.237. The curve of $C_{D_{ext,o-t}}$ was calculated as the difference between the faired curves of C_{D_T} and $C_{D_{i,o-e}}$ (using eq. (9) in coefficient form). In figures 19(a) and 19(b), the faired curves of $C_{D_{ext,o-t}}$ are shown for lips 0, 16R, and 18E for free-stream Mach numbers of 0.237 and 0.330, respectively. Figure 19 also includes the curves of calculated additive-drag coefficient and of external-body drag coefficient (calculated using eqs. (6) and (8), respectively, in coefficient form).

For the calculation of additive-drag coefficient for the inlet with lip 0, the stagnation streamline of the entering flow was assumed to terminate at the sharp leading edge. For lip 16R, the position of the stagnation point was found, approximately, from cross plots of surface-pressure-distribution data for the lip region. No static orifices were provided in lip 18E; however, since lips 16R and 18E provided similar contraction ratios, it was assumed that the variation of the additive-drag coefficient with mass-flow ratio was about equal for the two lips.

The sharp breaks in the curves of $C_{D_{ext,o-t}}$, which are repeated in the curves of external-body drag coefficient in figure 19, are believed to correspond with the occurrence of flow separation from the external surface of the lips. The dashed portions of the curves show the range of mass-flow ratios over which the drag measurements were

unsteady as a result of the separation. In particular, for the inlet with lip 18E for a Mach number of 0.330, the unsteadiness of forces for a mass-flow ratio slightly greater than 0.3 prevented accurate measurements. For lip 0, for mass-flow ratios less than 1.0, the external flow was separated at the lip at all times and there was, of course, no break in the drag-coefficient curves.

The drag coefficient of the solid body, indicated by the circle symbol at a mass-flow ratio of zero in figures 19(a) and 19(b), may be seen to agree closely with the external-body drag coefficient calculated for the ducted body with lip 0 for a mass-flow ratio of 1.00. A comparison of the drag coefficients for the solid body in figures 19(a) and 19(b) shows that there was a small decrease of drag with increasing Mach number. This was believed to have been a scale effect since, as the Mach number was increased from 0.237 to 0.330, the Reynolds number increased from about 136,000 to 185,000 per inch.

The variations of the internal-drag coefficient $C_{D_{i,o-e}}$ with mass-flow ratio for a given free-stream Mach number for the model with each of the three lips were found to be nearly identical. This equality would be expected in view of the fact that the total-pressure recovery and mass-flow characteristics with each of the lips (fig. 5) were similar for mass-flow ratios less than 1.0. It can be seen, then, from equation (9) in coefficient form, that the differences between the curves of $C_{D_{ext,o-t}}$ in figures 19(a) and 19(b) are a measure of the actual drag differences resulting from the use of the various lips. These curves show that none of the lips provided the lowest drag throughout the range of mass-flow ratios from 0 to 1.0 for the free-stream Mach numbers of the test. The greatest improvement in drag measured with lips 16R and 18E, compared with that measured with lip 0, occurred for the mass-flow ratios just before the external flow separated from the lips and also near a mass-flow ratio of zero.

Surface-pressure distribution.- The static pressure over the inlet and body was measured by means of one row of static-pressure orifices whose positions are tabulated in figures 1 and 2. Examples of the pressure-coefficient distributions plotted against $(r/r_{max})^2$ are included in figures 20(a) and 20(b) for lips 0 and 16R, respectively, for a free-stream Mach number of 0.237. It was found that the effect of mass-flow ratio on the pressure distribution was limited almost completely to the region near the inlet; therefore, figure 20 includes data only for $(r/r_{max})^2$ to 0.5. The area under the curves of the type illustrated, from the stagnation point to any arbitrary station, is equal to the external pressure-drag coefficient for the body to that station. The changes in the external pressure-drag coefficients with mass-flow ratio are plotted in figure 21. Similar differences for external-body drag coefficients $C_{D_{ext,s-t}}$ from force data (from figs. 19(a) and 19(b)) are also plotted in figure 21 for comparison with the pressure-drag coefficients. It can be seen that nearly the same

change of external-body drag with mass-flow ratio was obtained by each of the methods. This was particularly true for the case of lip 0.

Based on this agreement between pressure and force measurements, it is believed that the change of viscous drag with mass-flow ratio for the test conditions was small. Additional verification of this belief was obtained from approximate calculations of viscous drag based on the pressure distribution. Since the majority of the pressure changes with changing mass-flow ratio took place near the inlet and ahead of the station at which transition was fixed, the calculated viscous drag was found to be essentially constant.

Relation of external-body drag to additive drag.- Ideal potential flow theory (ref. 1) shows that for mass-flow ratios below 1.0, the change of calculated additive drag with mass-flow ratio should be of equal magnitude but of opposite sign to the change of inlet lip suction forces. For the present tests, the change of inlet lip suction force with mass-flow ratio is expressed in figure 21 as the change in external-body drag coefficient. For comparison, the change of additive-drag coefficient calculated for lips 0, 16R, and 18E is also included in figure 21. To simplify the comparison, additive-drag coefficient is considered in the negative sense. It can be seen in figure 21 that, for lip 0, the change in the two coefficients was equal only for mass-flow ratios approaching 1.0. For the other two lips, they were approximately equal over the range of mass-flow ratios for which the external flow was believed to have remained attached to the lip surfaces.

CONCLUSIONS

The following conclusions pertaining to the effects of inlet lip bluntness and profile on diffuser performance and body drag are based on the results of tests conducted, with a body of revolution having a circular nose inlet, for free-stream Mach numbers up to 0.33 and for inlet flows from zero through choking:

1. For lips of moderate bluntness, an elliptical profile provides better pressure recovery than a circular profile.

2. For choking flow in the inlet with either sharp or blunt lips, large total-pressure fluctuations may exist in a diffuser. The amplitude of the fluctuations measured in this investigation was as great as 15 percent of the free-stream total pressure and the frequency was of the order of 20 cycles per second or less.

3. For mass-flow ratios less than 1.0, the magnitude of the change of external drag of the body with a change of mass-flow ratio is, in accordance with potential theory, equal but of opposite sign to the

change of the calculated additive drag for the inlet, as long as the external flow is not separated from the lip.

Ames Aeronautical Laboratory
National Advisory Committee for Aeronautics
Moffett Field, Calif., Jan. 9, 1954

REFERENCES

1. Coale, Charles W.: Suction Force on the Lip of a Two-Dimensional Idealized Scoop in Non-Viscous Subsonic Flow. Douglas Aircraft Co., Inc., Rep. SM-13742, Apr. 1950.

2. Sibulkin, Merwin: Theoretical and Experimental Investigation of Additive Drag. NACA RM E51B13, 1951.

3. Klein, Harold: The Calculation of the Scoop Drag for a General Configuration in a Supersonic Stream. Douglas Aircraft Co., Rep. SM-13744, Apr. 1950.

4. Fradenburgh, Evan A., and Wyatt, DeMarquis D.: Theoretical Performance Characteristics of Sharp-Lip Inlets at Subsonic Speeds. NACA TN 3004, 1953.

5. Staff of the Ames Aeronautical Laboratory: Equations, Tables, and Charts for Compressible Flow. NACA Rep. 1135, 1953. (Formerly NACA TN 1428)

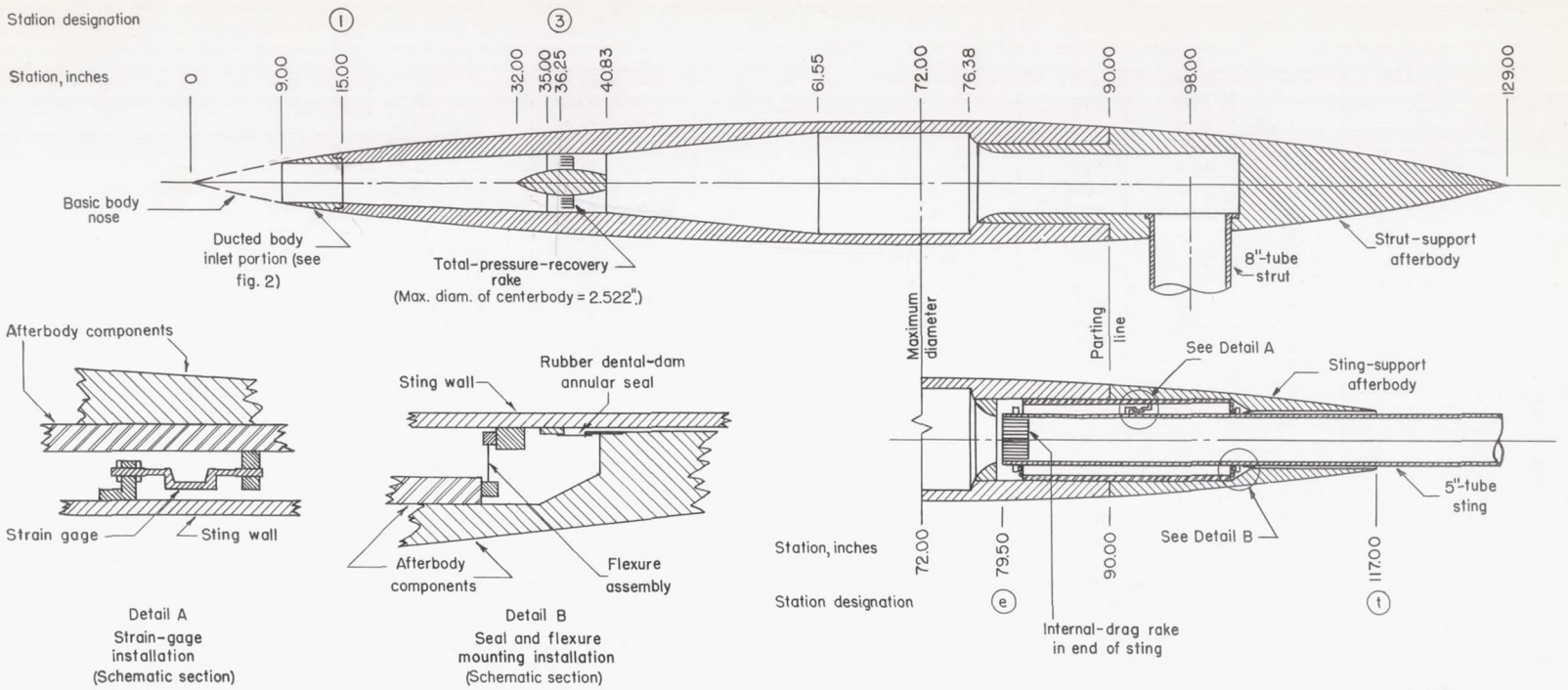

Detail A
Strain-gage installation
(Schematic section)

Detail B
Seal and flexure mounting installation
(Schematic section)

External ordinates, forebody			
Station	Radius	Station	Radius
0	0	49.00	5.535
9.00	2.022(1) / 2.078(2)	59.00	5.852
14.118	2.753	69.00	5.992
19.00	3.342	72.00	6.000
24.00	3.858	78.00	5.950
29.00	4.308	81.00	5.900
34.00	4.695	84.00	5.820
39.00	5.028	90.00	5.530

(1) Basic body
(2) Ducted body

External ordinates, afterbody		
Station	Radius	
	Strut-support configuration	Sting-support configuration
90.00	5.530	5.530
96.00	5.120	5.140
101.00	--	4.670
102.00	4.560	(3)
108.00	3.870	(3)
114.00	3.100	(3)
117.00	2.625	2.625
120.00	2.050	
126.00	0.730	
129.00	0	

Internal ordinates	
Station	Radius
9.00	2.078
15.00	2.078
35.00	2.822
40.83	2.822
61.55	5.000
76.38	5.000

(3) Sting-support afterbody is conical between stations 101.00 and 117.00.

Static-pressure orifices on sting-supported model at stations:	
16.2	73.8
23.4	81.0
30.6	88.2
37.8	95.4
45.0	99.0
52.2	109.8
59.4	115.25
66.0	

NACA

Figure 1.- Model details.

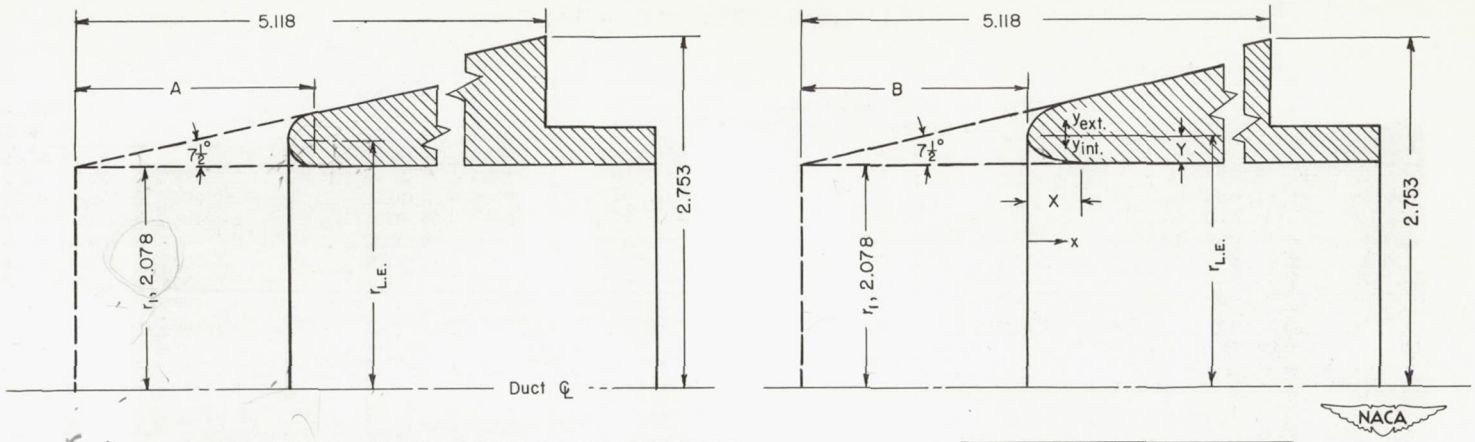

Circular lip dimensions				
Lip designation	Lip radius	A	$r_{L.E.}$	Contraction ratio $r^2_{L.E.}/r_1^2$
0	0	0	2.078	1.000
4 R	0.04	0.61	2.118	1.037
8 R	0.08	1.22	2.158	1.078
16 R	.16	2.44	2.238	1.158
24 R	.24	3.65	2.318	1.243
33 R	.32	4.88	2.398	1.330

Elliptical lip dimensions Y/X=0.2777		
Lip designation	8E	18E
Contraction ratio	1.078	1.177
Y	0.080	0.176
X	0.288	0.632
B	1.130	2.500
$r_{L.E.}$	2.158	2.254

Lip coordinates		
x/X	y/Y	
	Internal	External
0	0	0
0.007	0.120	0.133
.019	.194	.227
.037	.267	.314
.046	.300	.352
.111	.460	.534
.185	.580	.695
.259	.675	.809
.333	.747	.911
.445	.834	1.031
.556	.894	1.128
.704	.954	
.741	.962	
.852	.988	
1.000	1.000	

Static-pressure orifices at stations:	
Lip 0	Lip 16R
9.24 external	11.54 internal
9.49 "	11.44 "
9.74 "	11.36 "
9.98 "	11.28 L.E.
10.24 "	11.36 external
10.98 "	11.44 "
11.72 "	11.54 "
12.47 "	12.04 "
13.70 "	12.46 "
13.95 "	13.03 "
	13.57 "

All dimensions in inches unless otherwise noted.

Figure 2.- Inlet details.

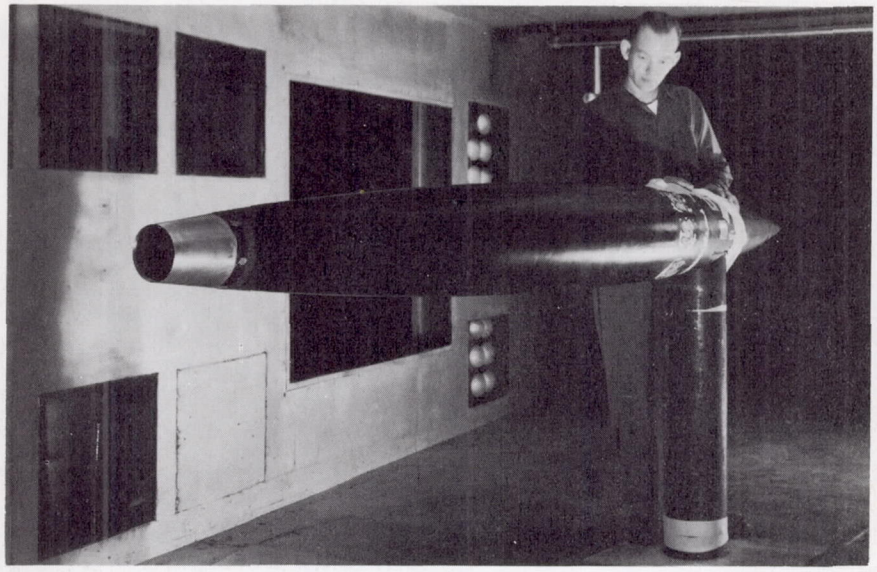

A-17024

(a) Strut-supported model.

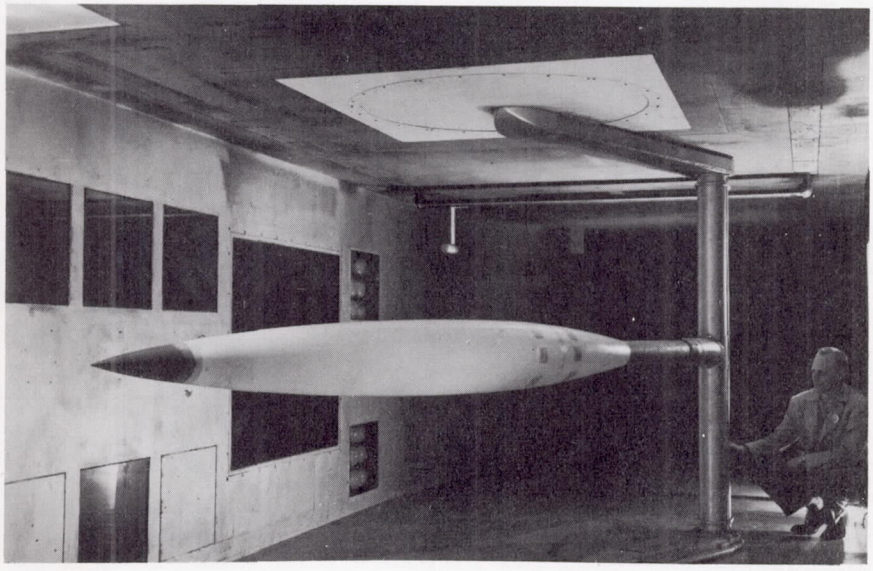

A-16916

(b) Sting-supported model.

Figure 3.- Photographs of model installed in 7- by 10-foot wind tunnel.

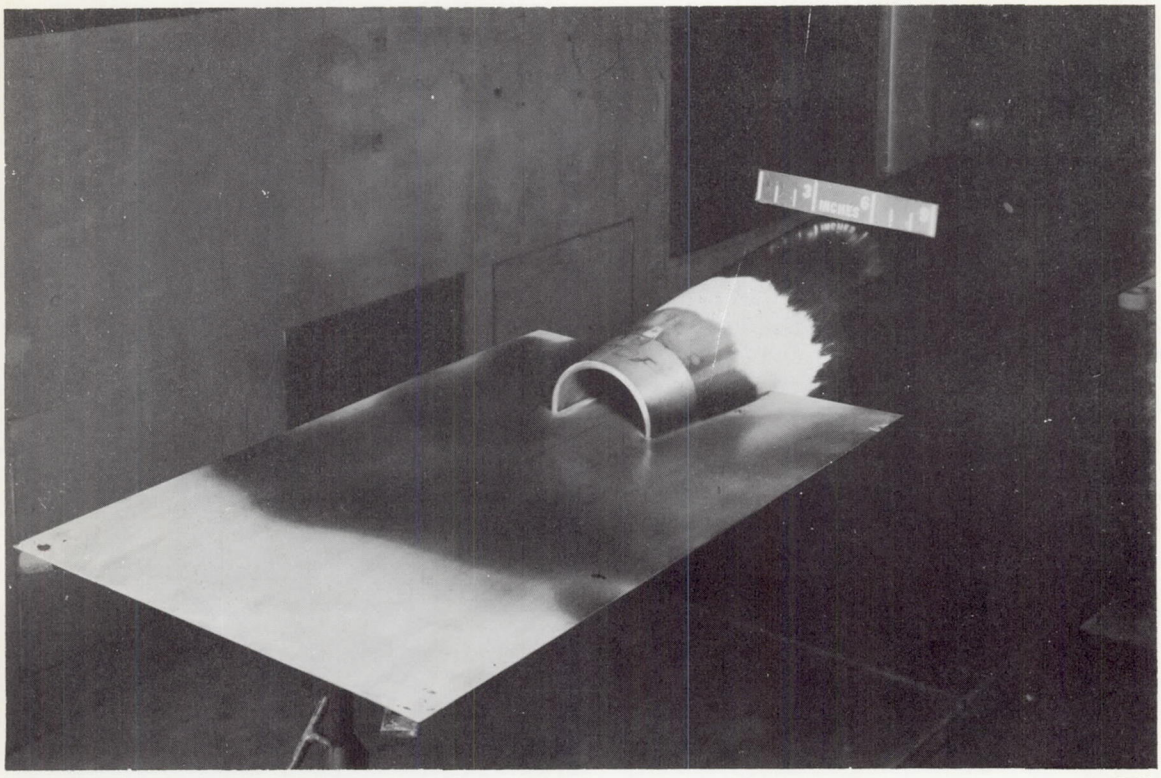

A-17100

Figure 4.- Flow study setup. Lip 16R.

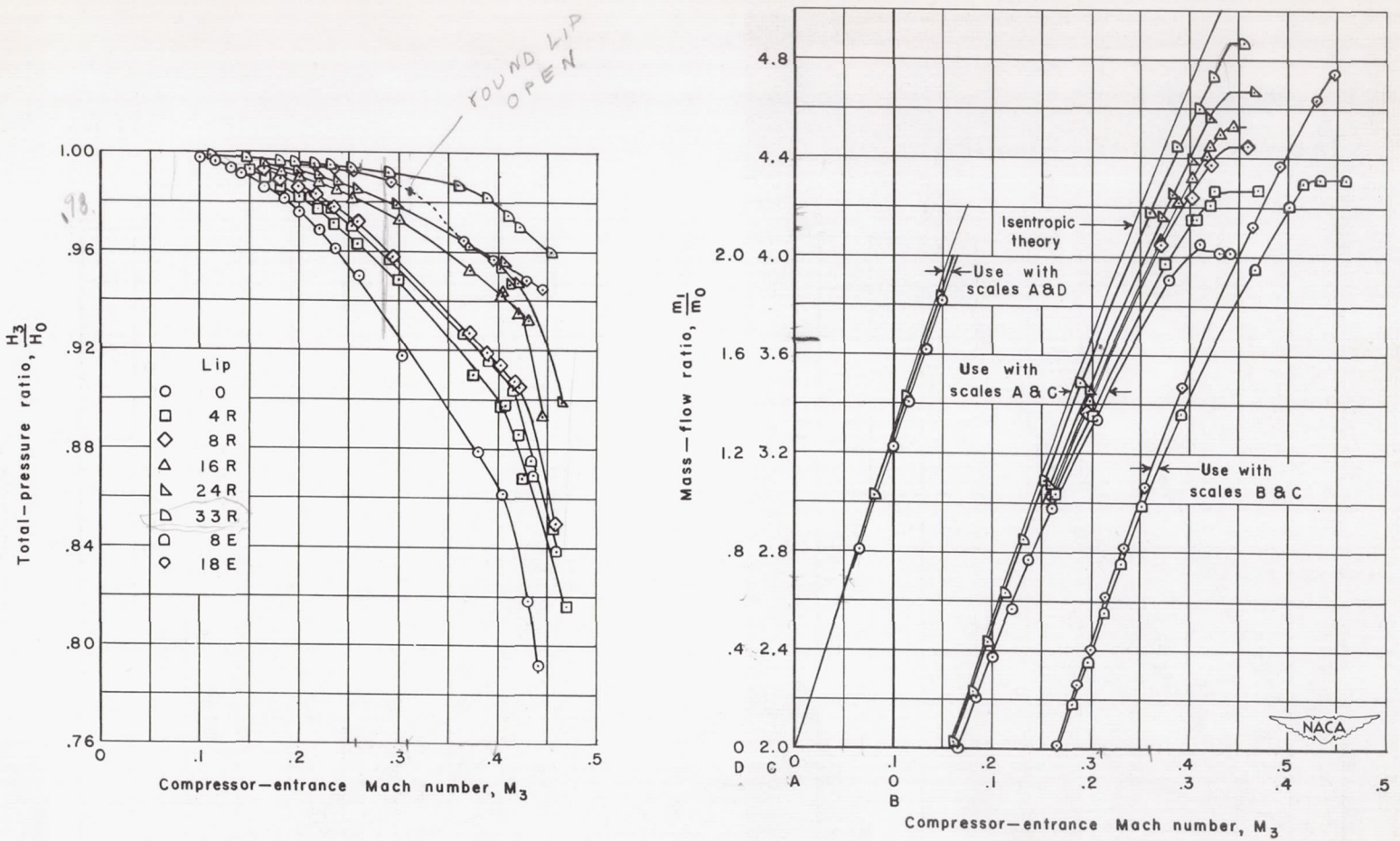

(a) $M_O = 0.115$

Figure 5.- The variations of total-pressure ratio and mass-flow ratio with compressor-entrance Mach number for each of the lips.

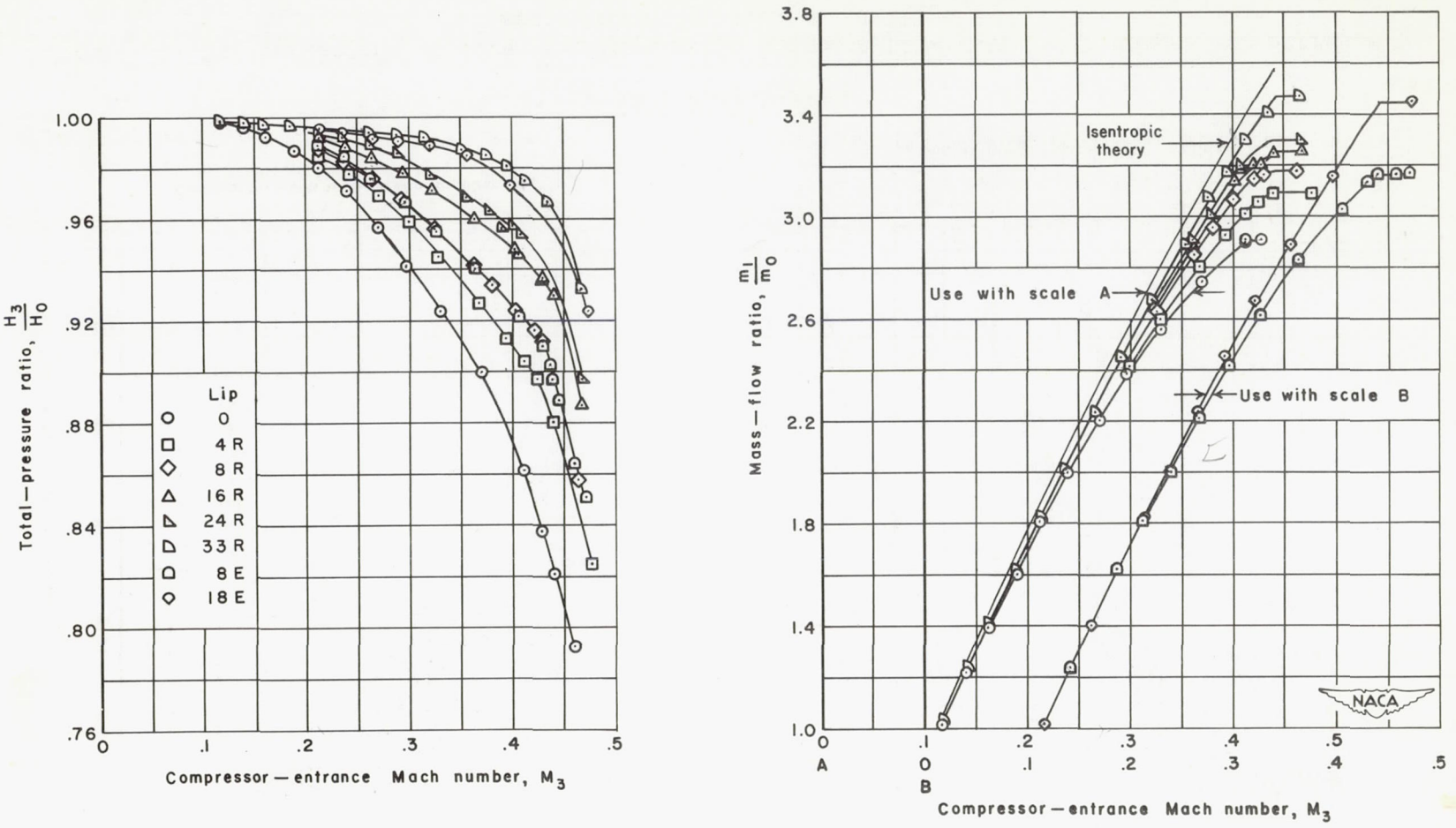

(b) $M_0 = 0.166$

Figure 5.- Continued.

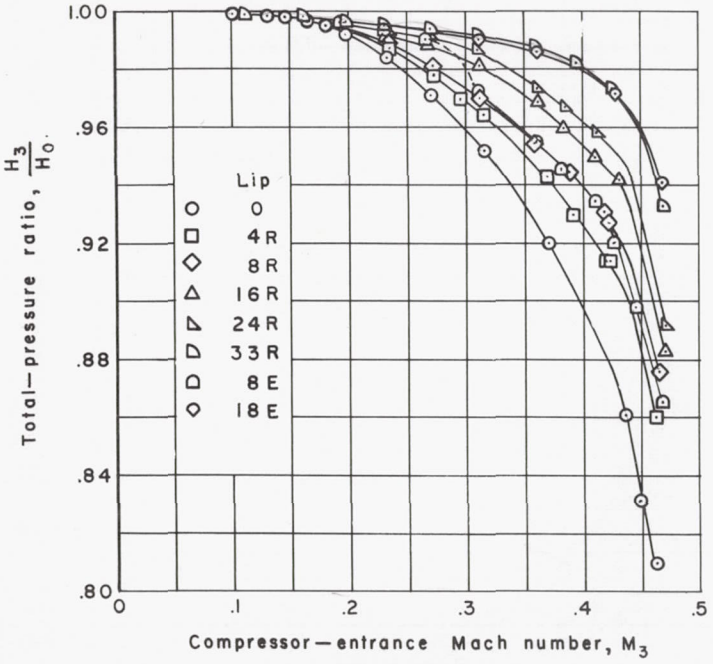

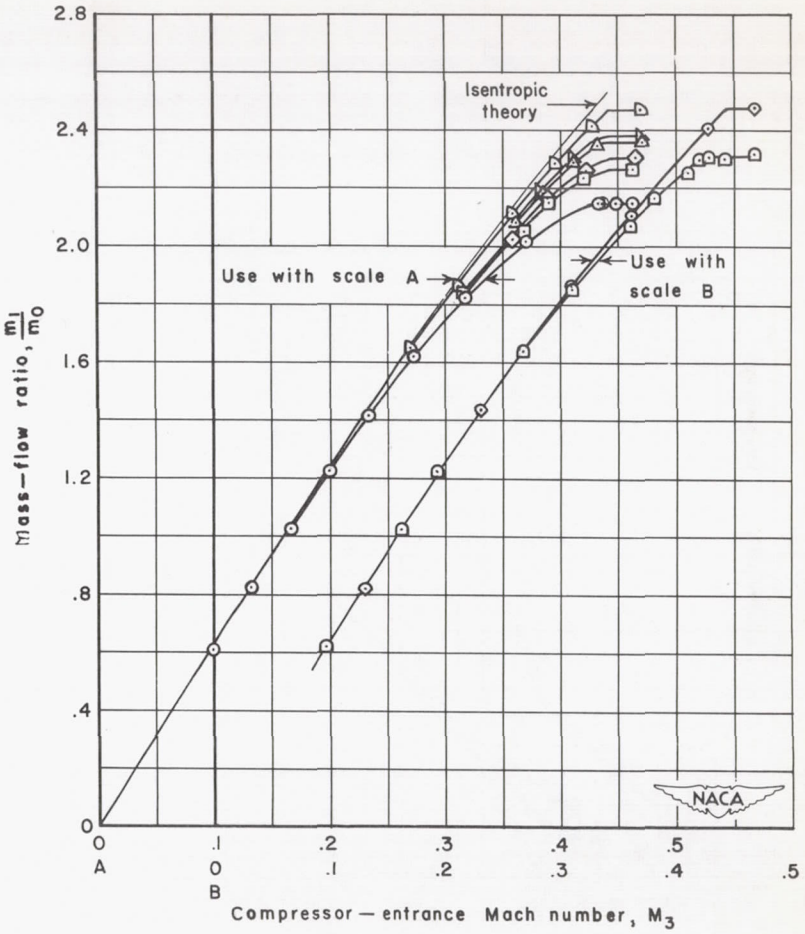

(c) $M_0 = 0.237$

Figure 5.- Continued.

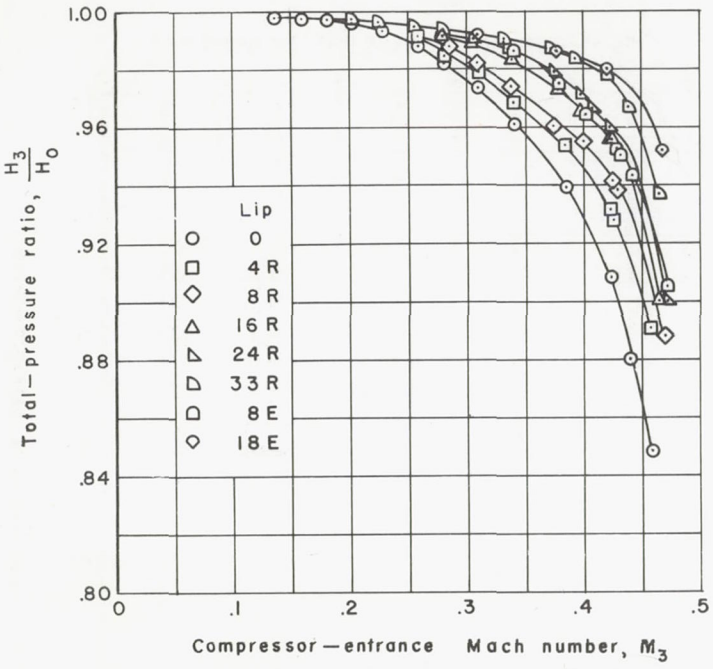

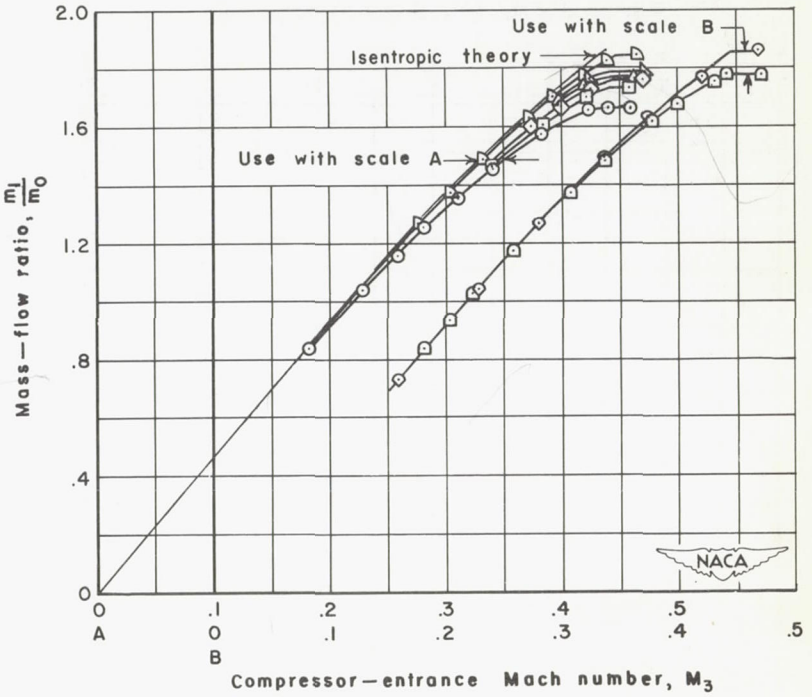

(d) M = 0.330

Figure 5.- Concluded.

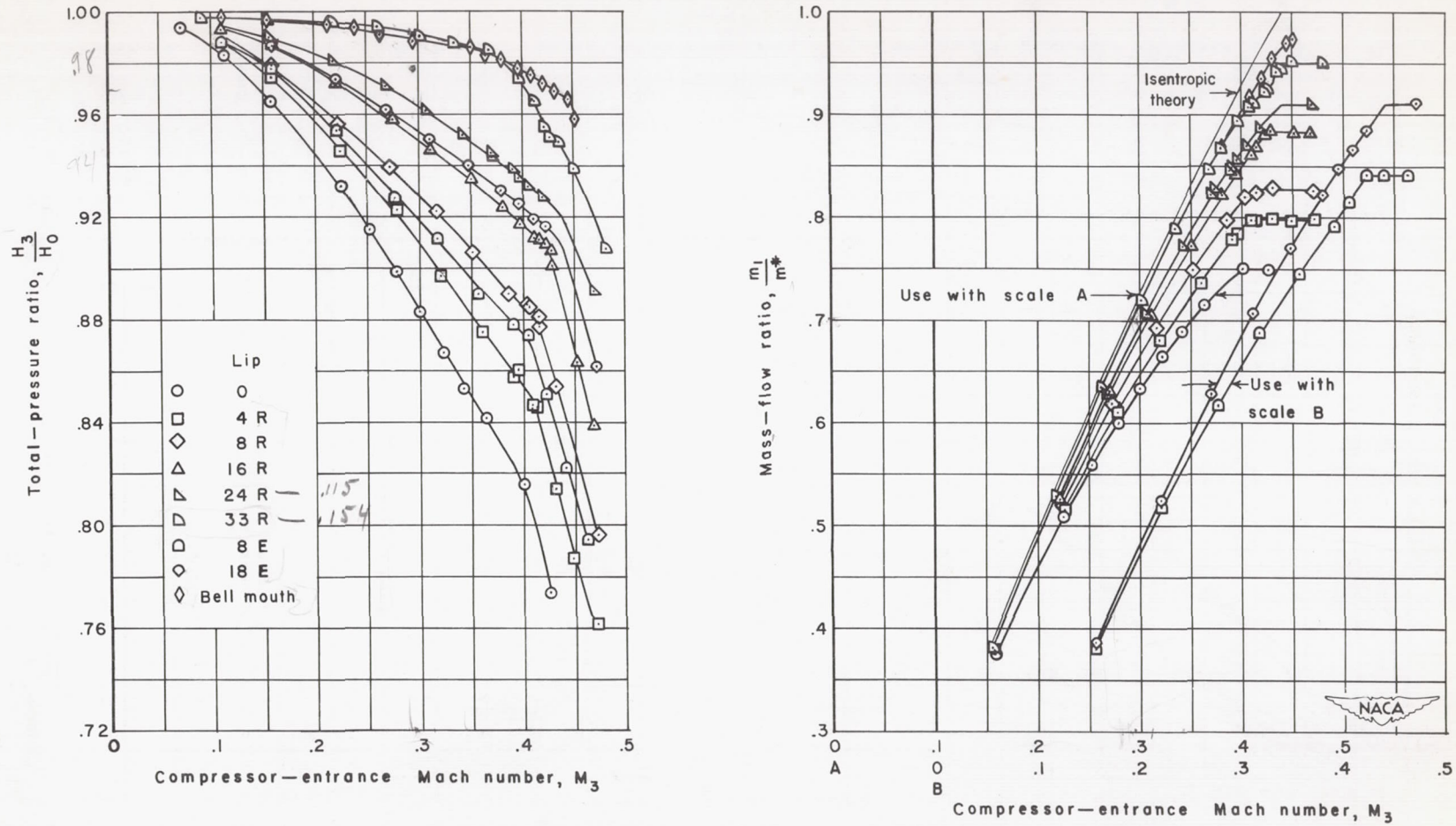

Figure 6.- The variations of total-pressure ratio and mass-flow ratio with compressor-entrance Mach number for each of the lips; $M_0 = 0$.

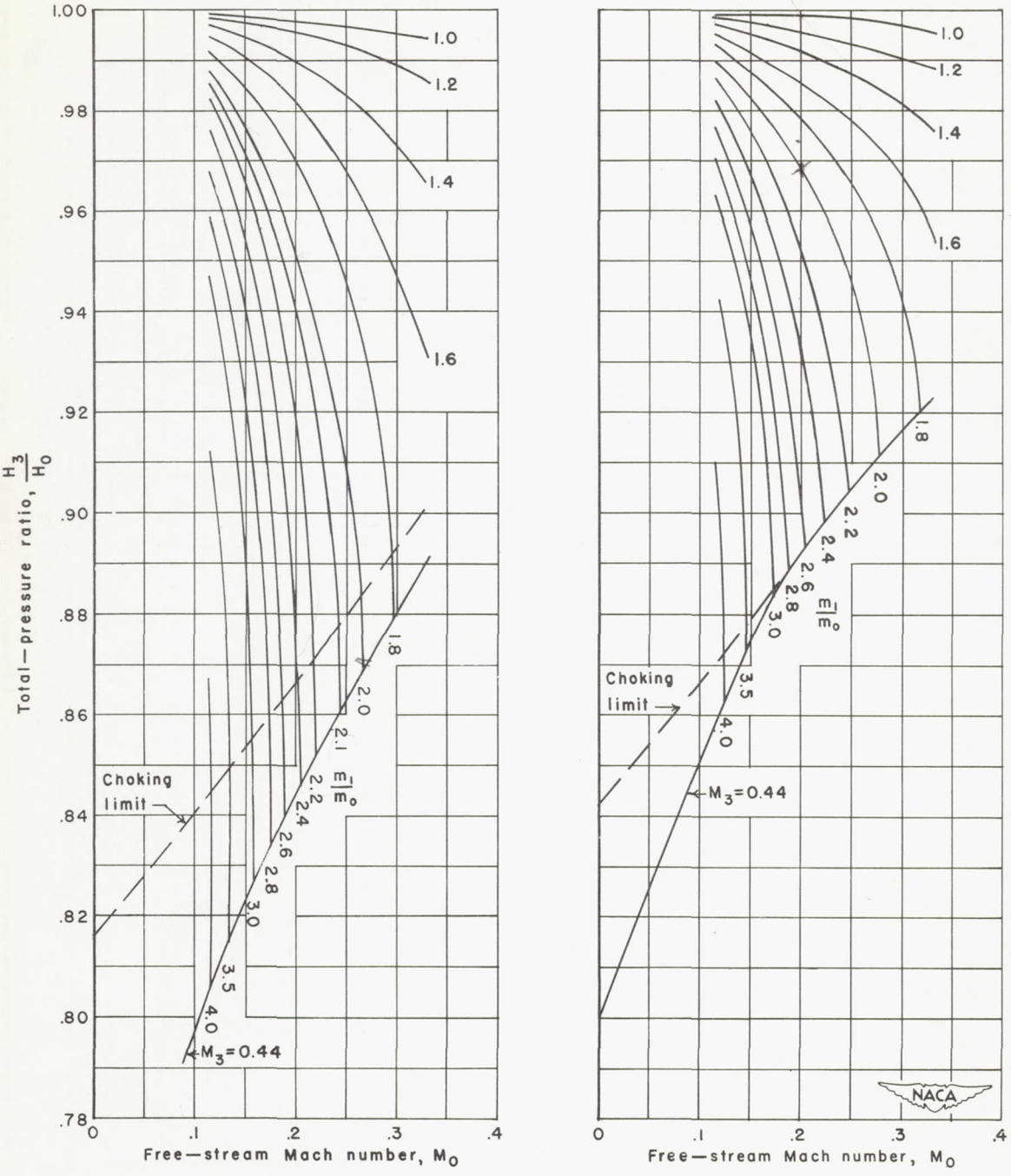

(a) Lip 0. (b) Lip 4R.

Figure 7.- The variation of total-pressure ratio with free-stream Mach number.

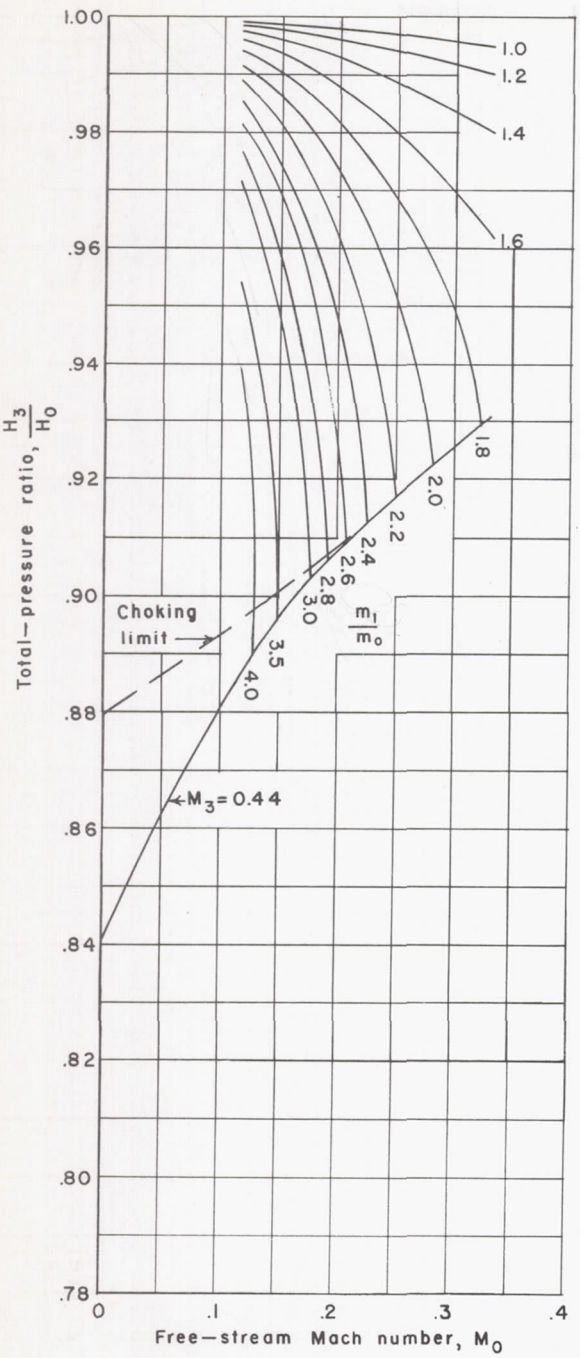

(c) Lip 8R.

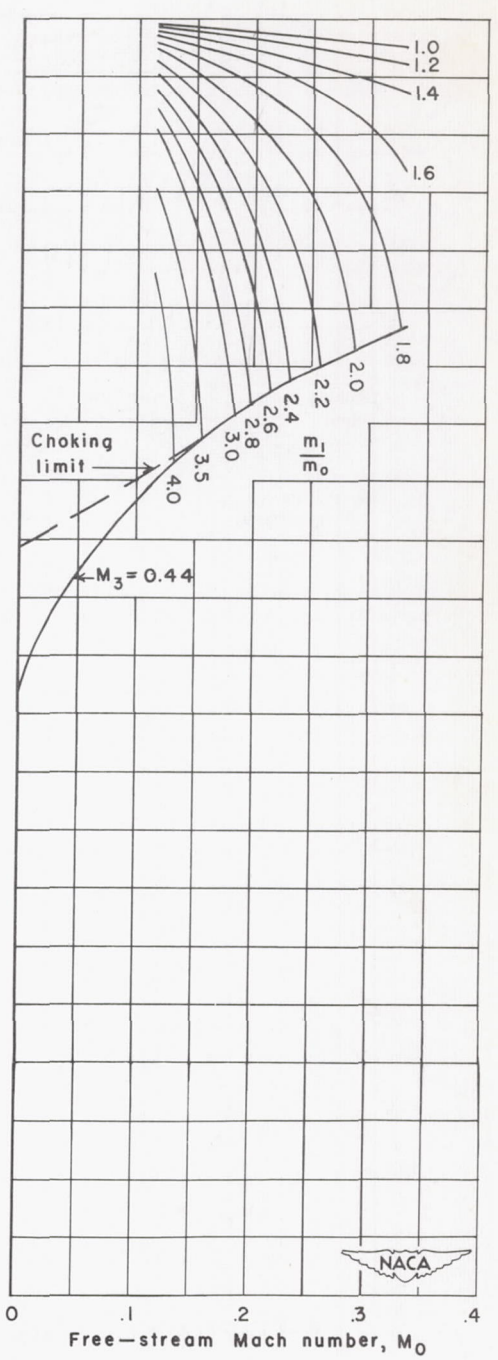

(d) Lip 16R.

Figure 7.- Continued.

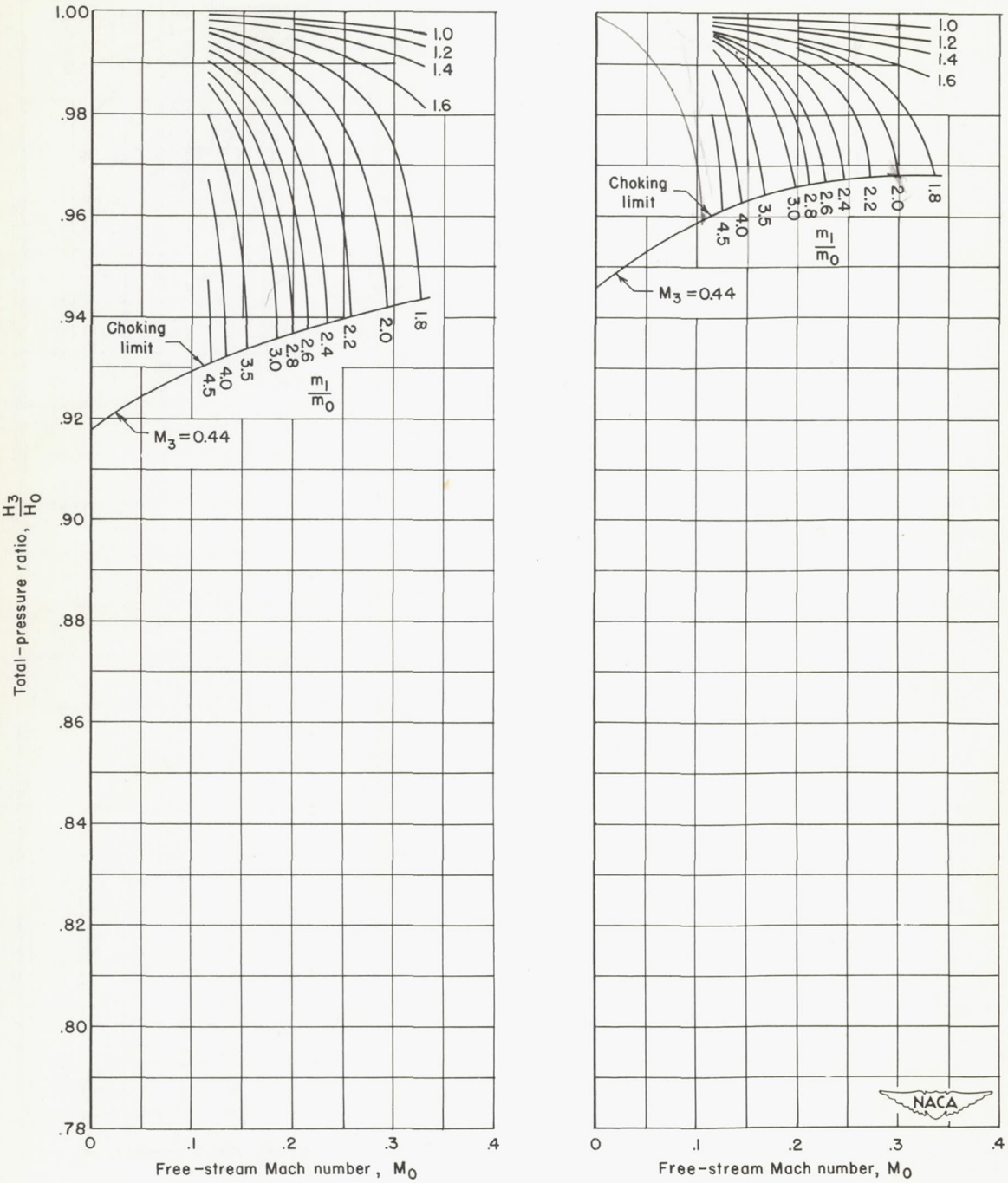

(e) Lip 24R. (f) Lip 33R.

Figure 7.- Continued.

3170

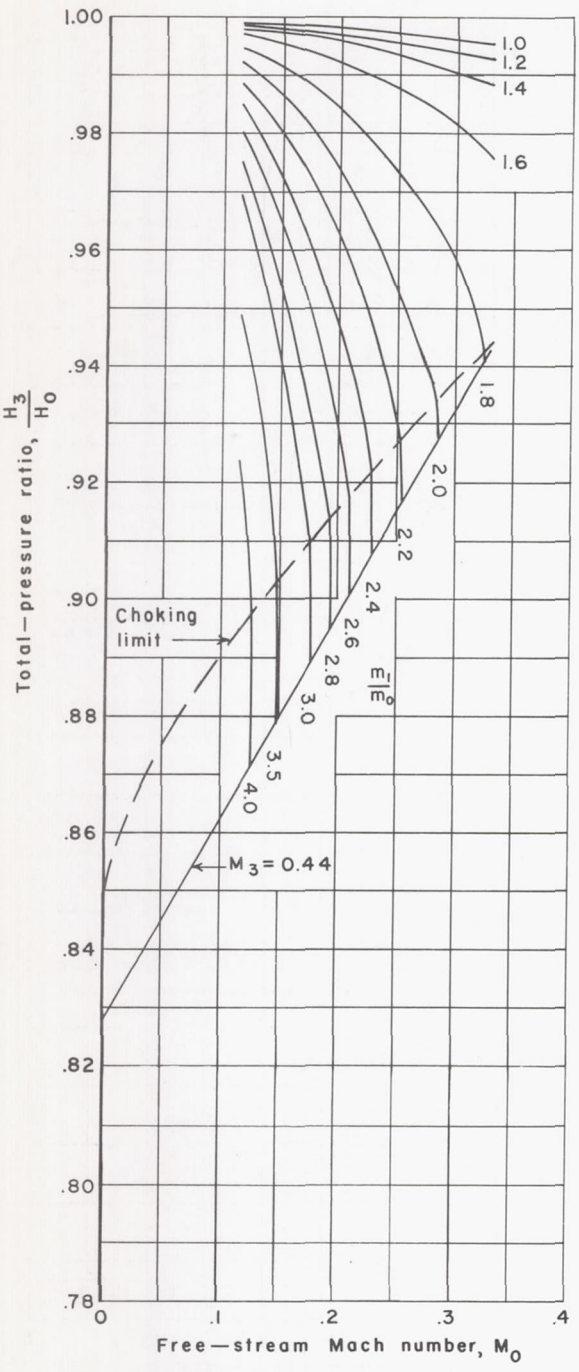

(g) Lip 8E.

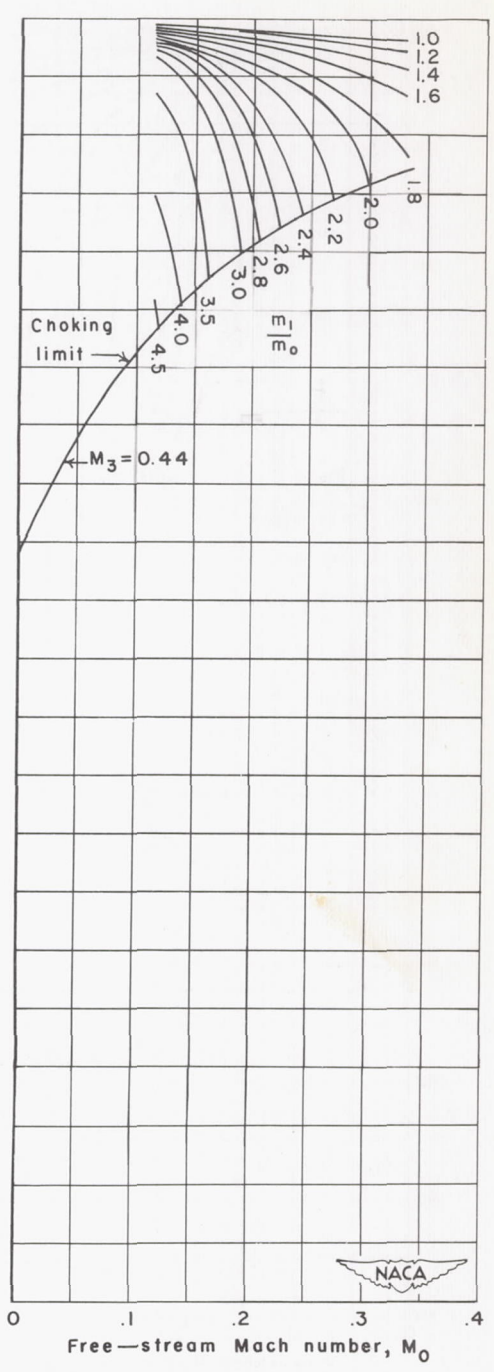

(h) Lip 18E.

Figure 7.- Concluded.

9933

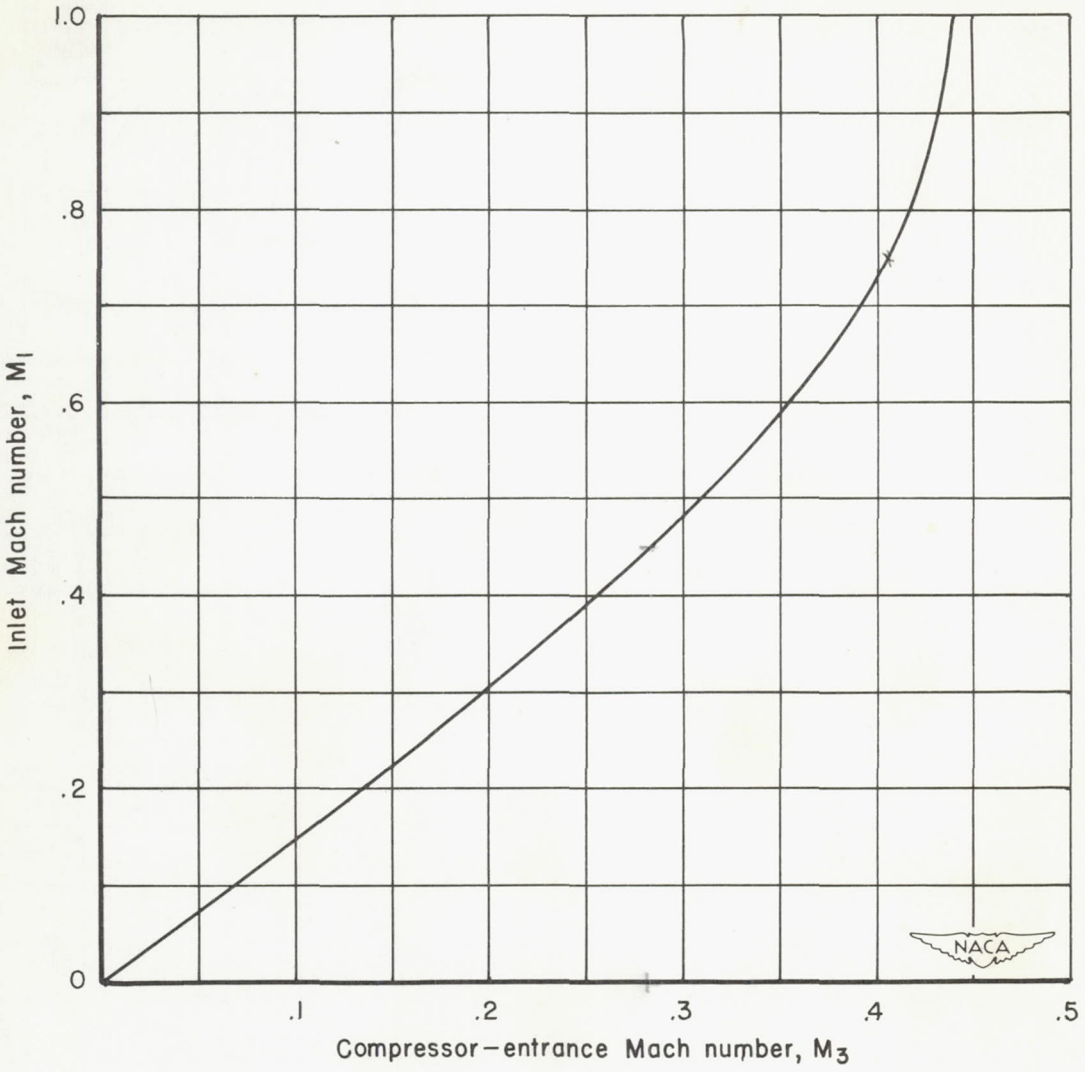

Figure 8.- The variation of inlet Mach number M_1 with compressor-entrance Mach number M_3 for isentropic flow.

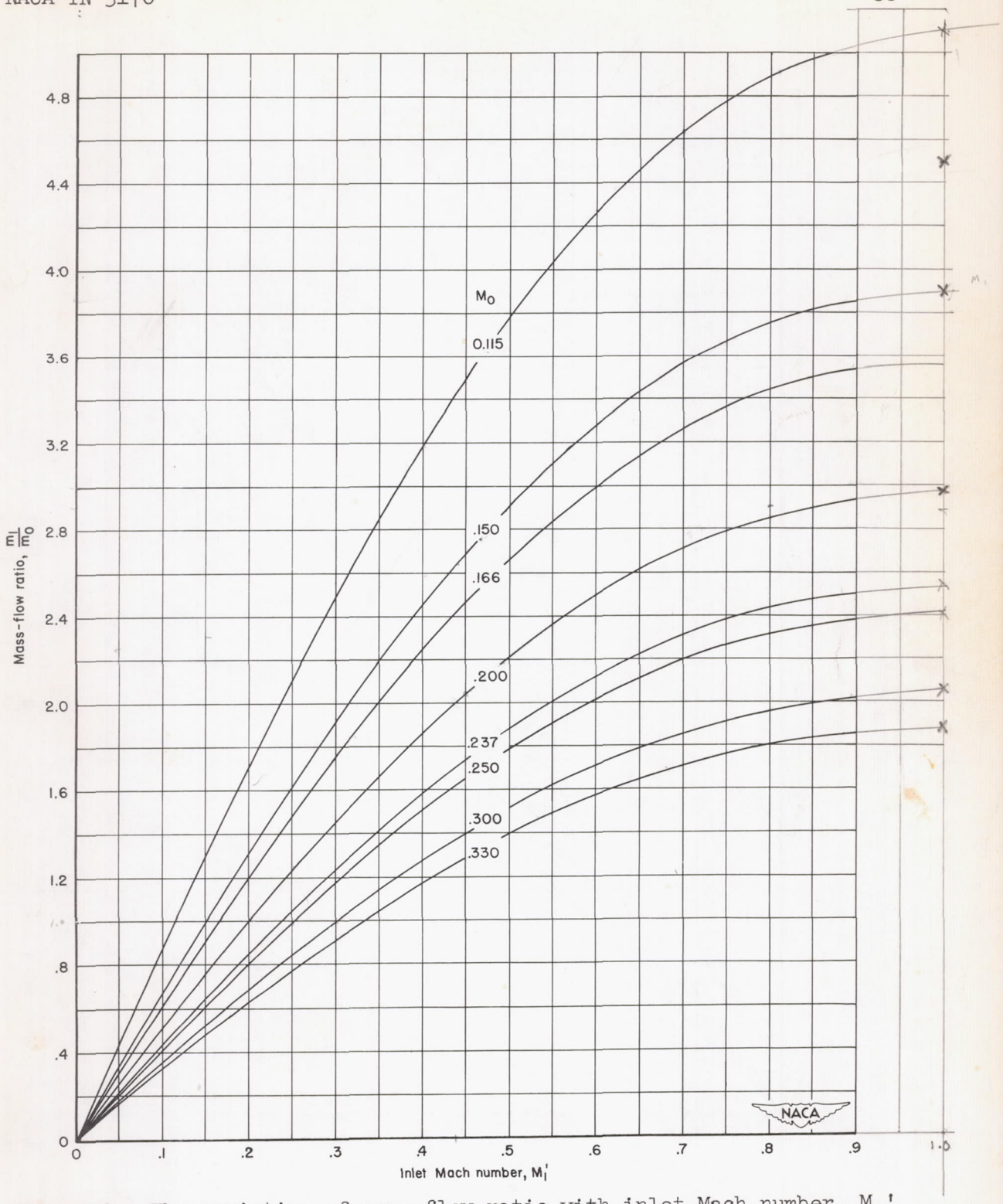

Figure 9.- The variation of mass-flow ratio with inlet Mach number M_1' and free-stream Mach number M_0 for isentropic flow.

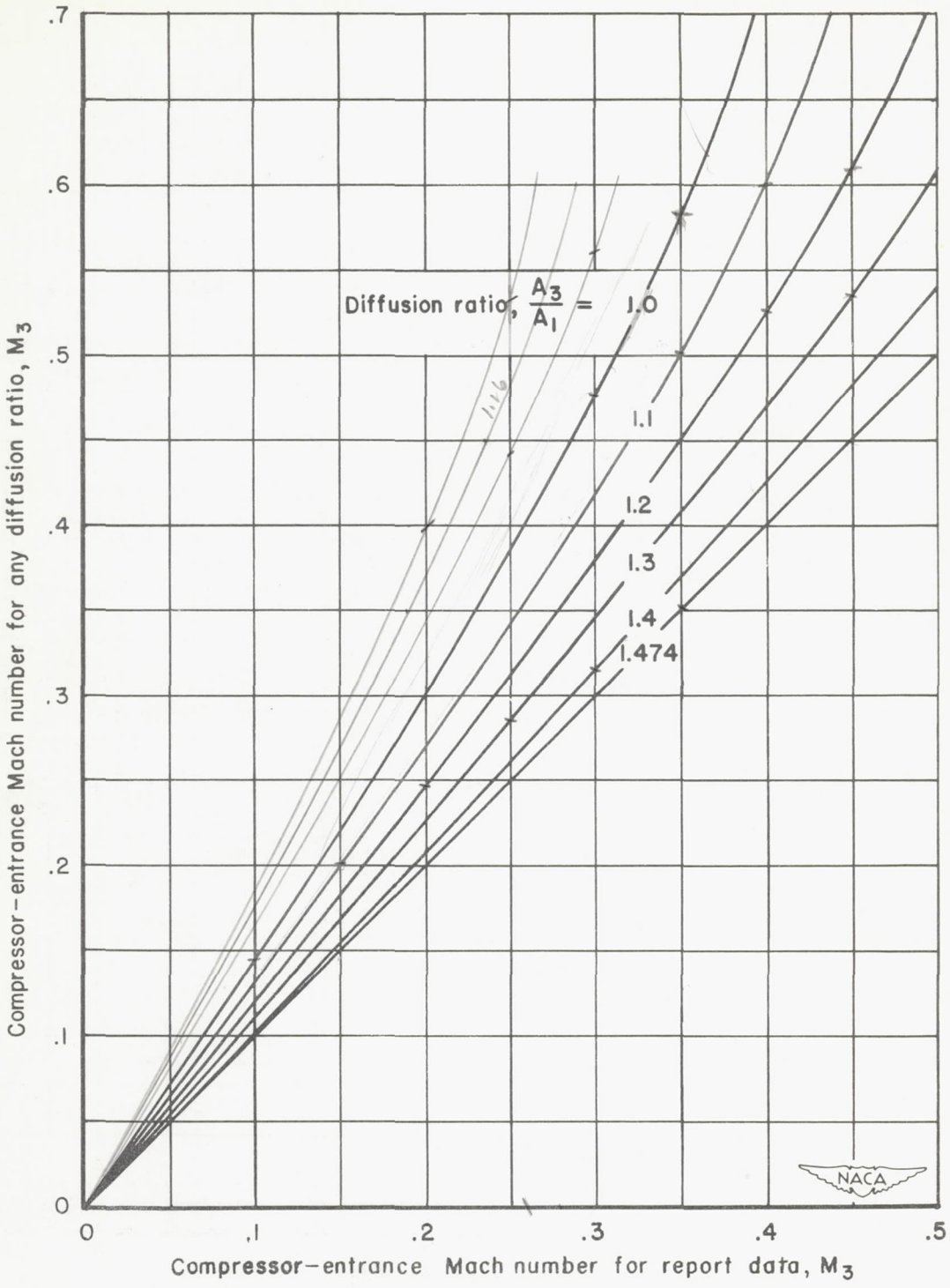

Figure 10.- Conversion curves to facilitate application of present test data to air-induction systems with other diffusion ratios.

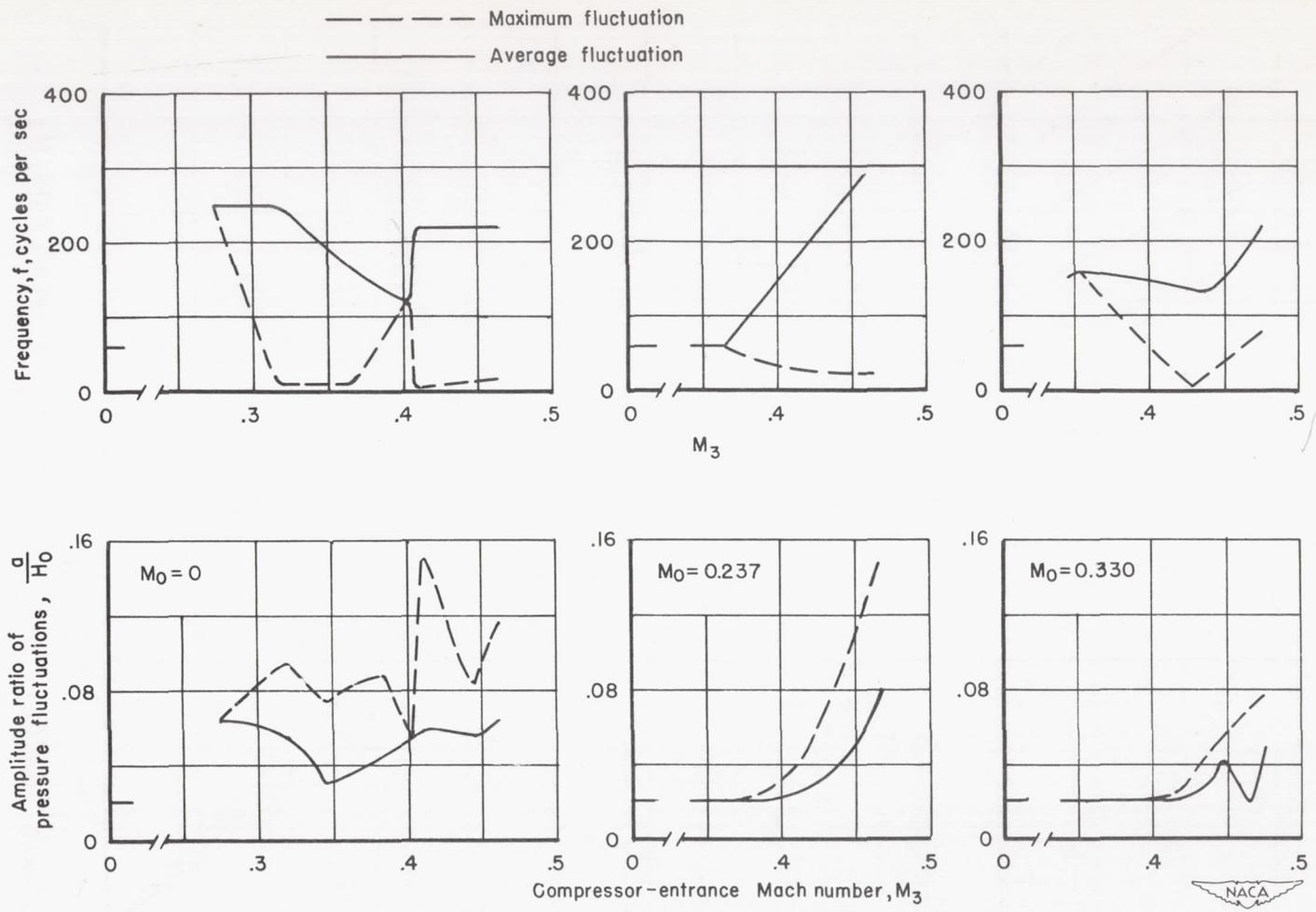

(a) Lip 0.

Figure 11.- Amplitude and frequency of total-pressure fluctuations in the diffuser.

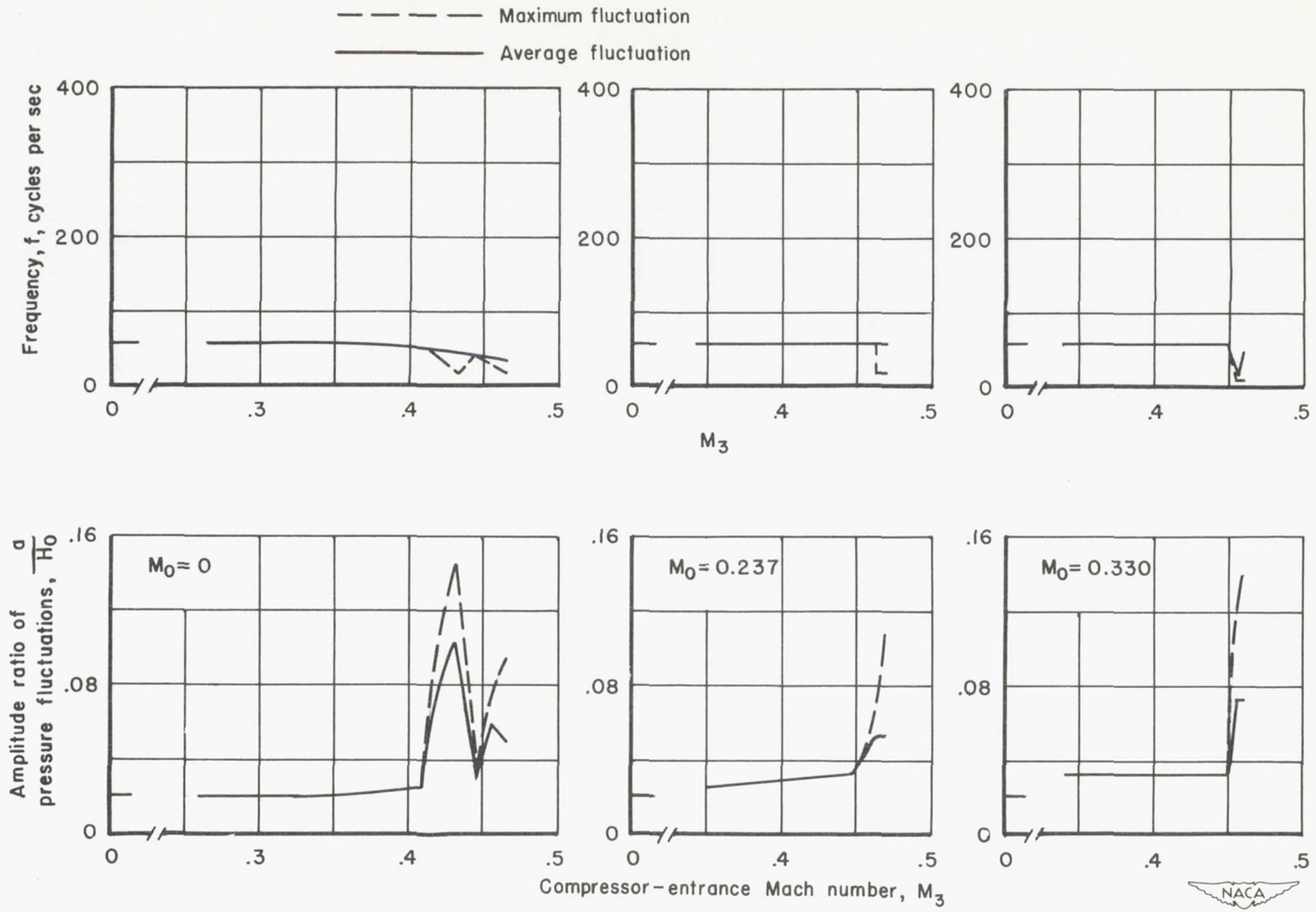

(b) Lip 16R.

Figure 11.- Concluded.

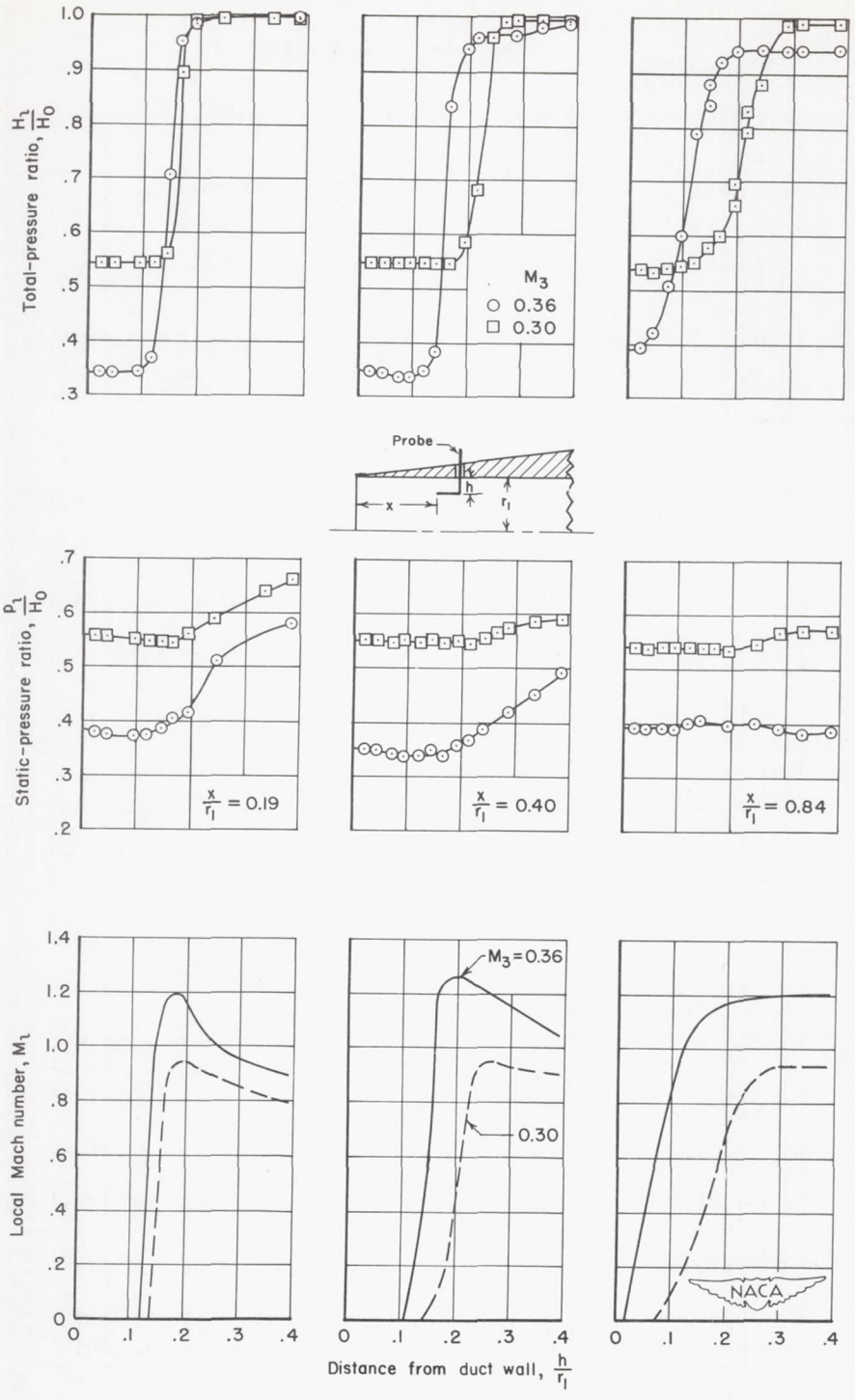

(a) Lip 0.

Figure 12.- The variations of local total- and static-pressure ratios and local Mach number with distance from the duct wall for stations in the inlet portion with lips 0 and 16R; $M_0 = 0$.

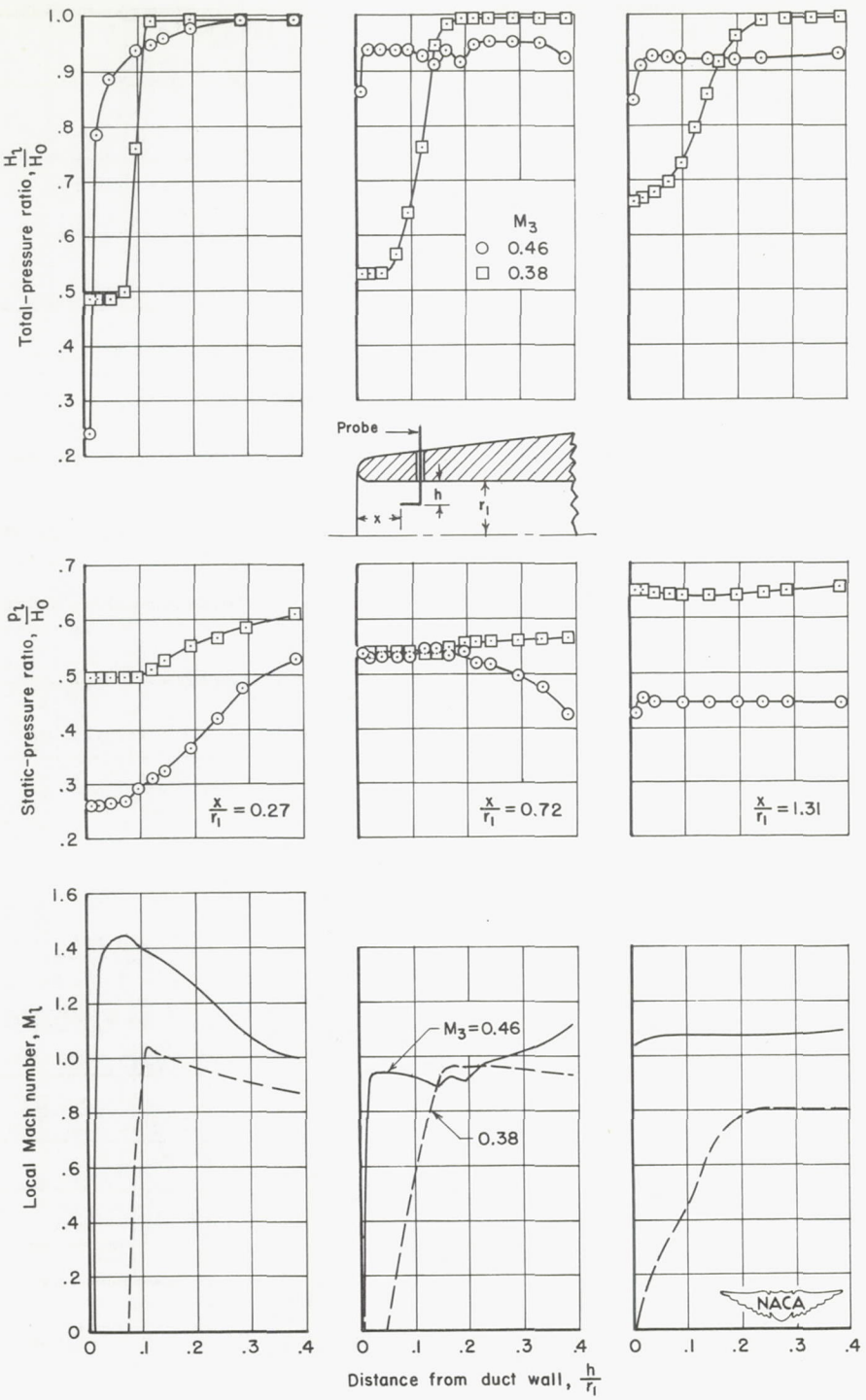

(b) Lip 16R.

Figure 12.- Concluded.

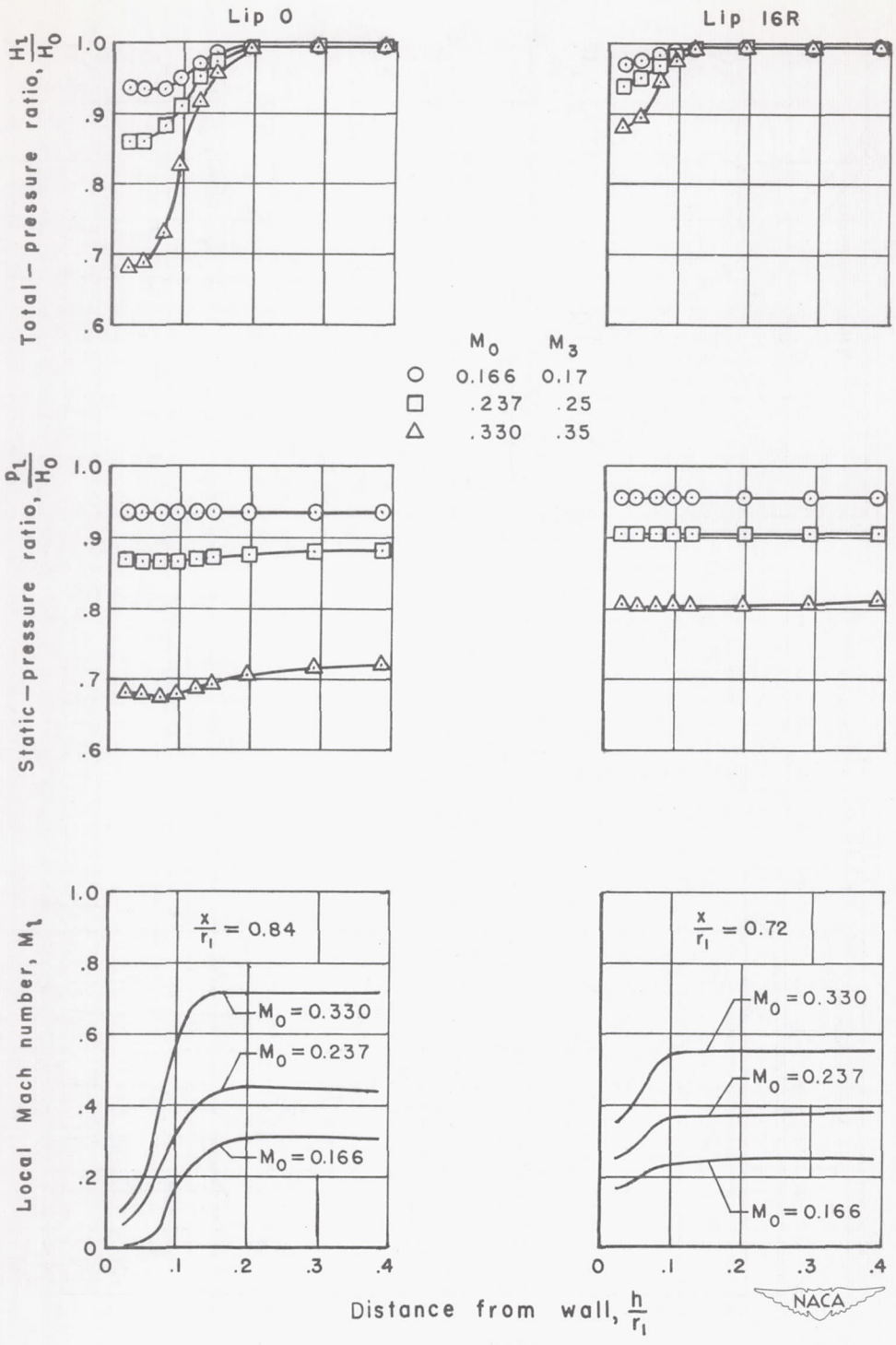

Figure 13.- The variations of the local static- and total-pressure ratios, and local Mach number with distance from wall of the inlet for several values of free-stream Mach number; $\frac{m_1}{m_0} \approx 1.5$.

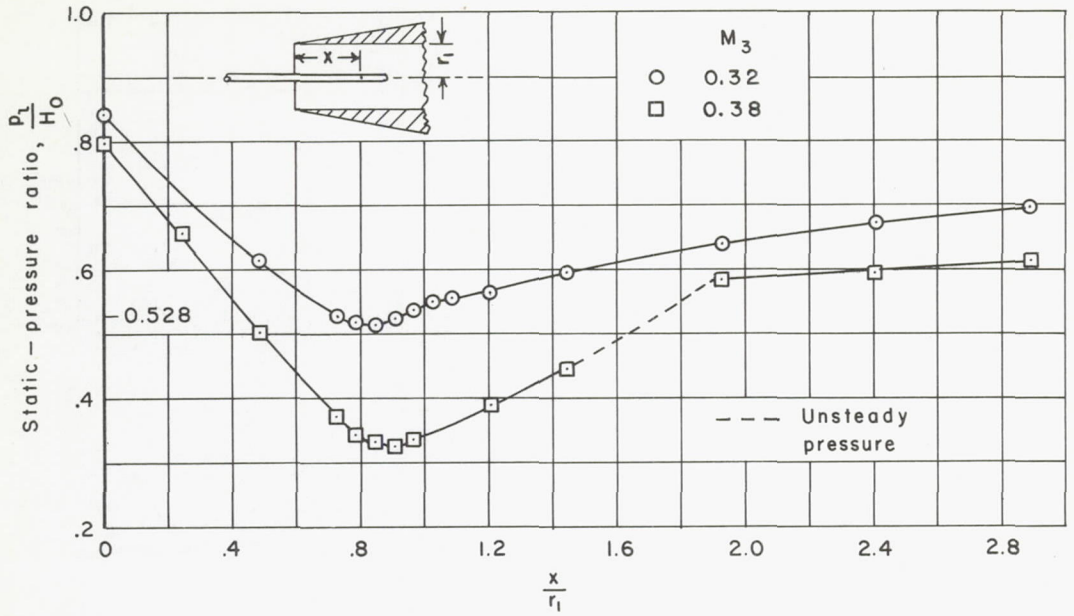

(a) Lip 0.

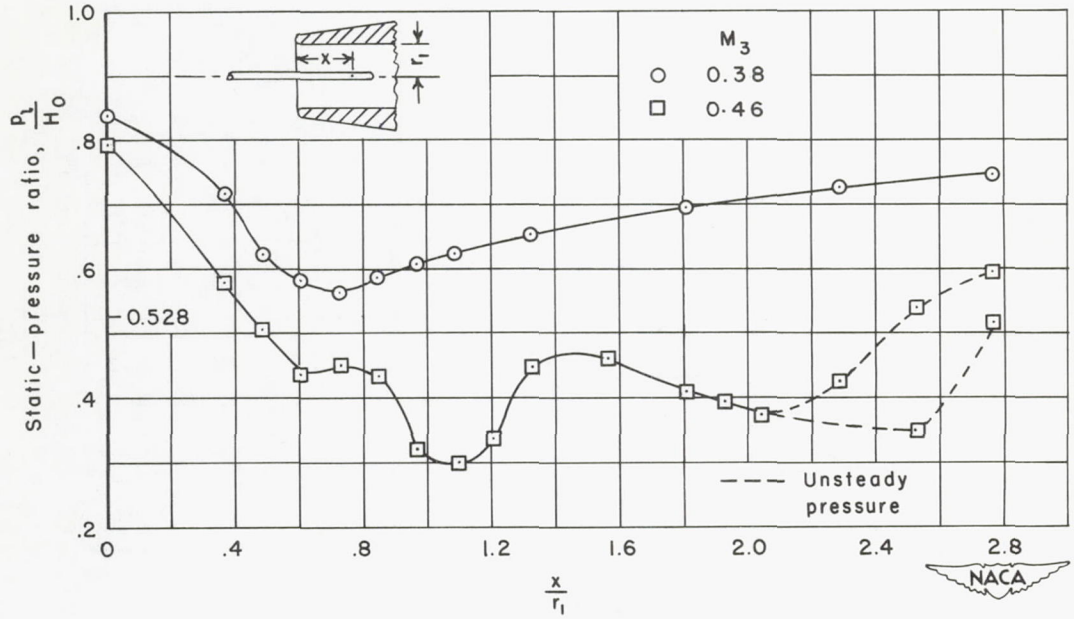

(b) Lip 16R.

Figure 14.- Static-pressure ratios along the center line of the inlet portion of the duct; $M_0 = 0$.

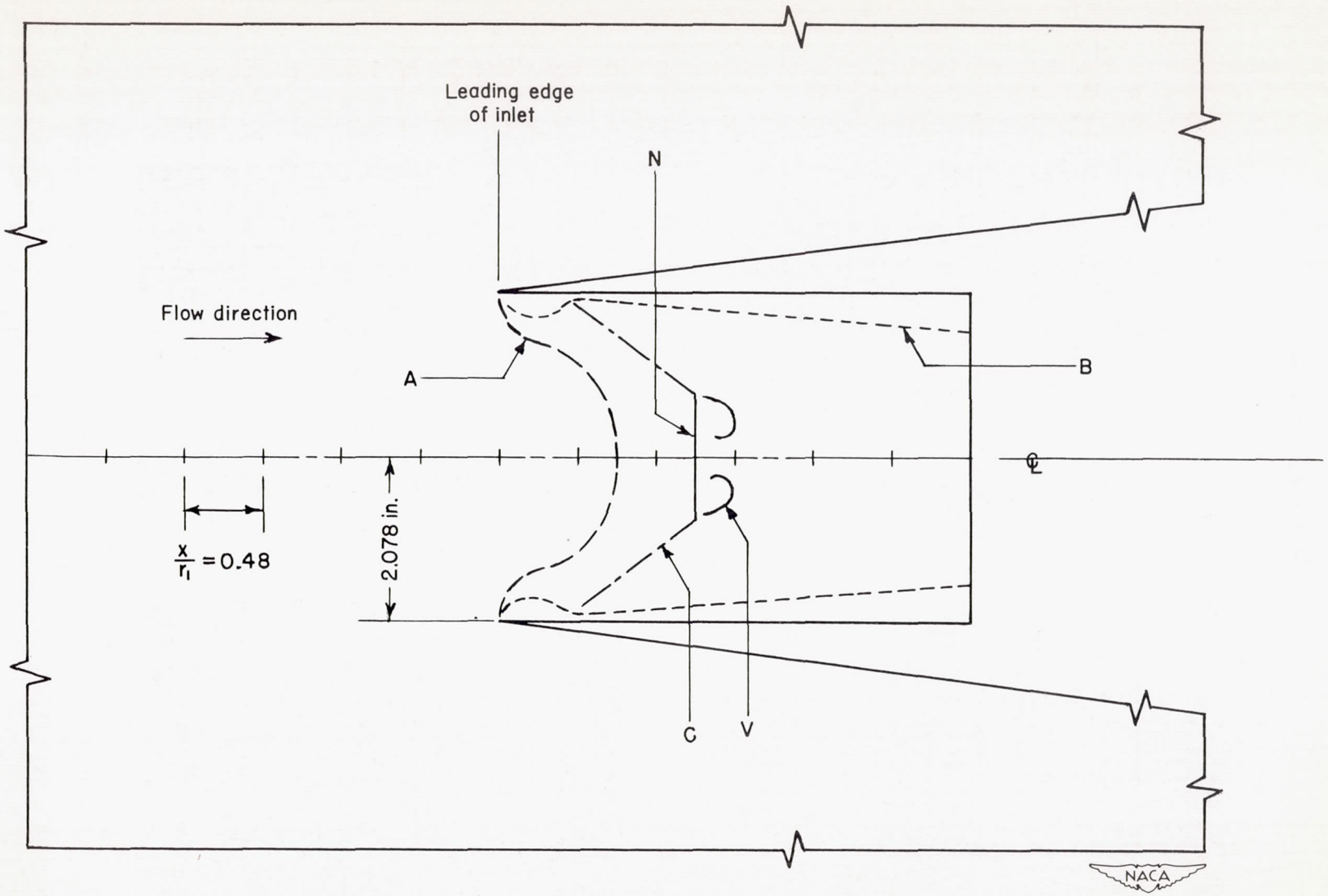

Figure 15.- Schematic representation of flow pictures.

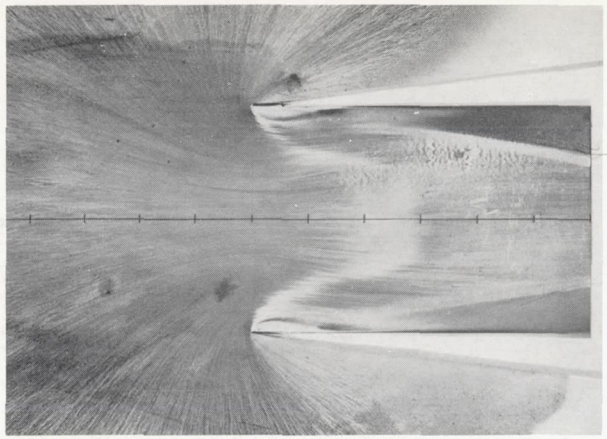

(a) $M_3 \approx 0.30$

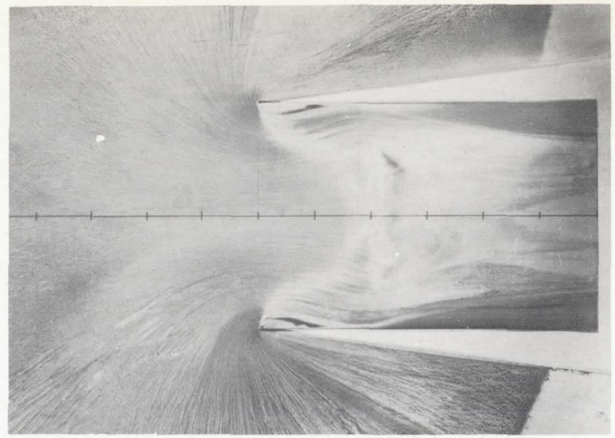

(b) $M_3 \approx 0.36$

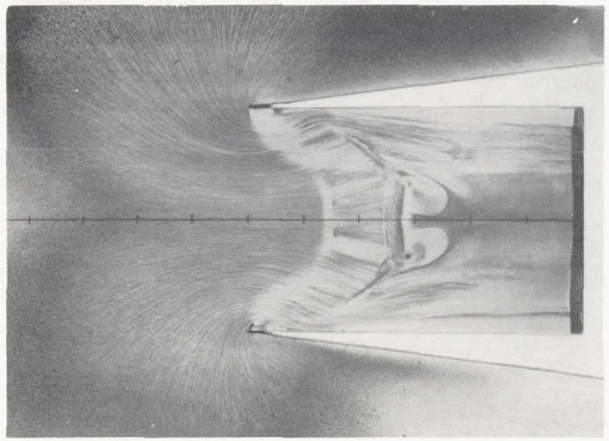

(c) $M_3 \approx 0.41$

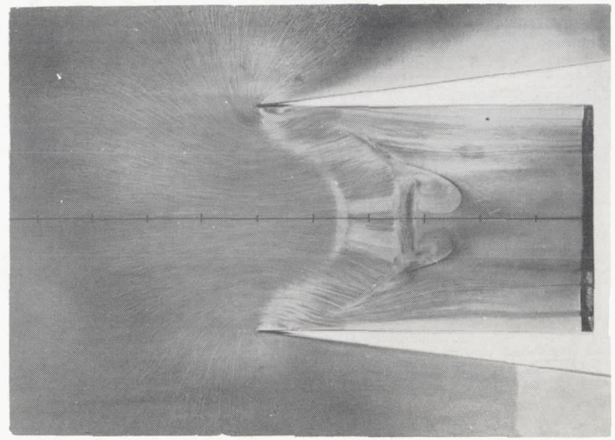

A-19029

(d) $M_3 \approx 0.44$

Figure 16.- Flow studies with lip 0; $M_0 = 0$.

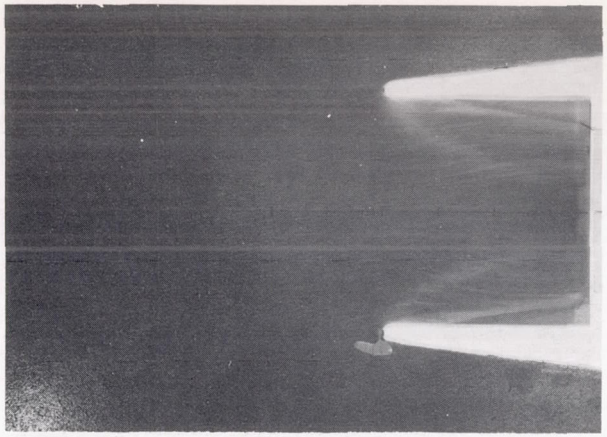

(a) $M_3 \approx 0.29$

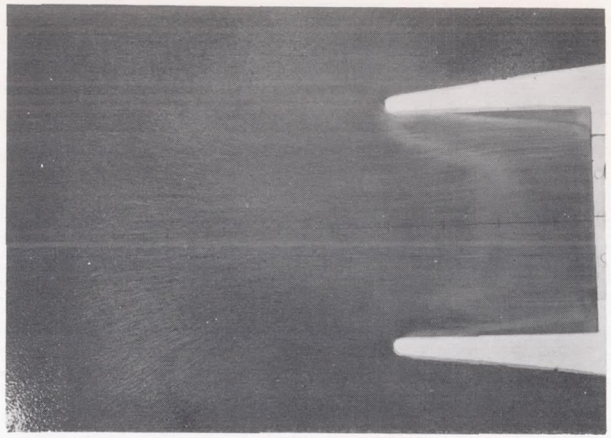

(b) $M_3 \approx 0.38$

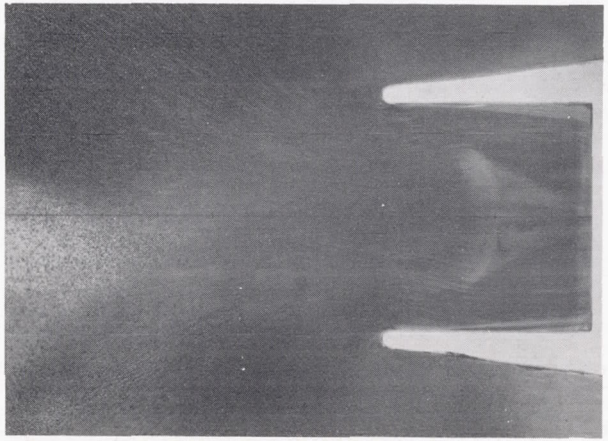

(c) $M_3 \approx 0.41$

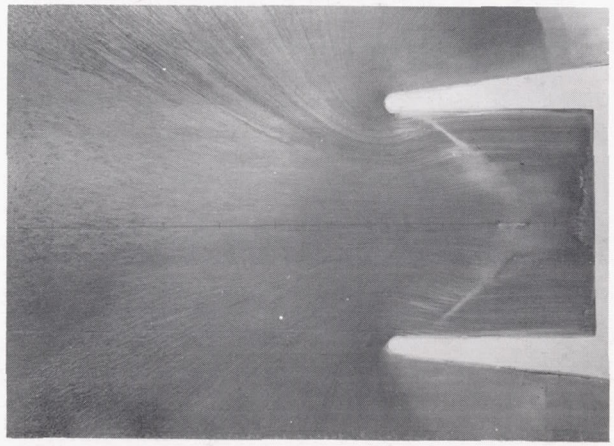

(d) $M_3 \approx 0.47$

A-19030

Figure 17.- Flow studies with lip 16R; $M_0 = 0$.

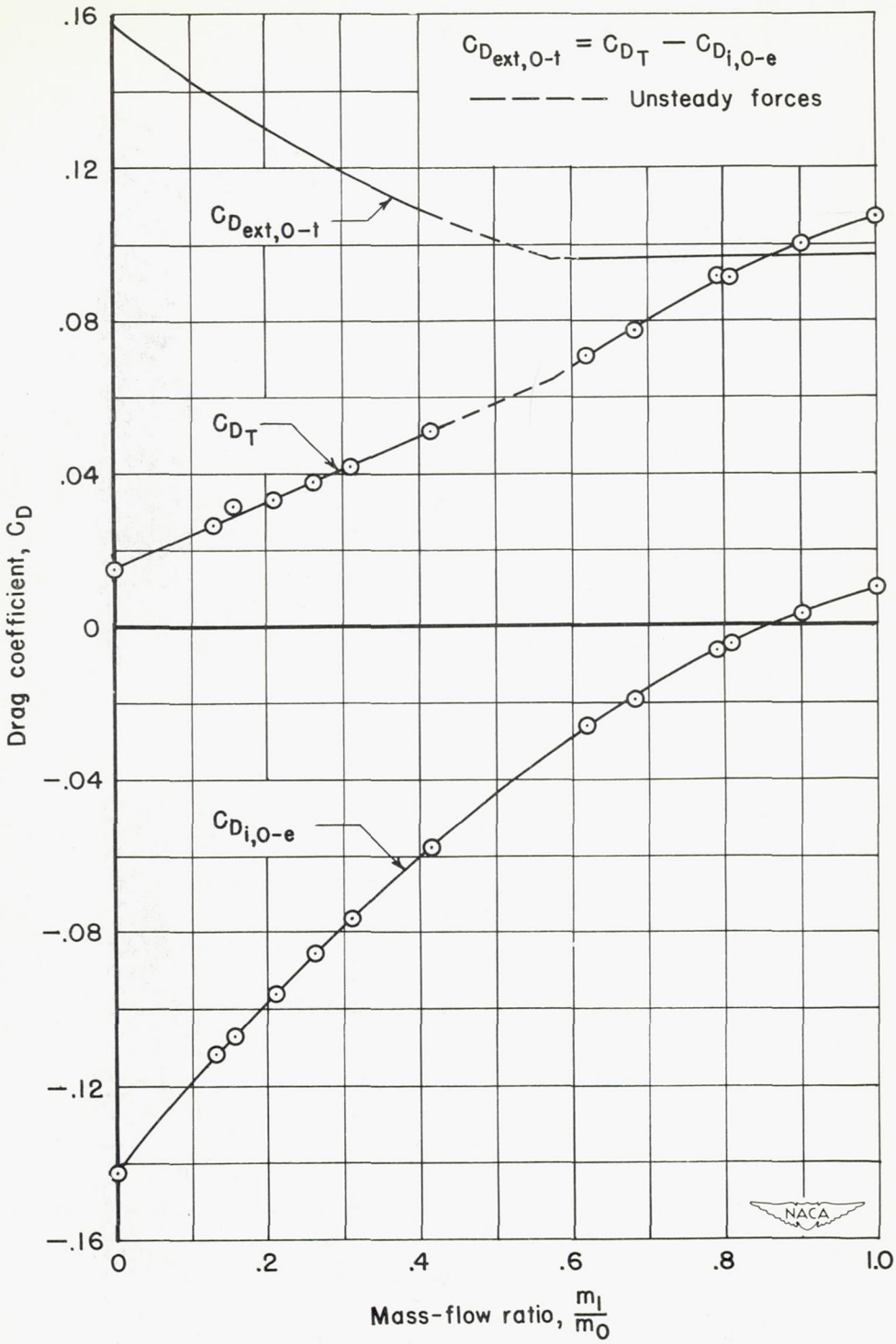

Figure 18.- Sample plot showing the total-drag coefficient and its components as a function of mass-flow ratio; Lip 18E, $M_O = 0.330$.

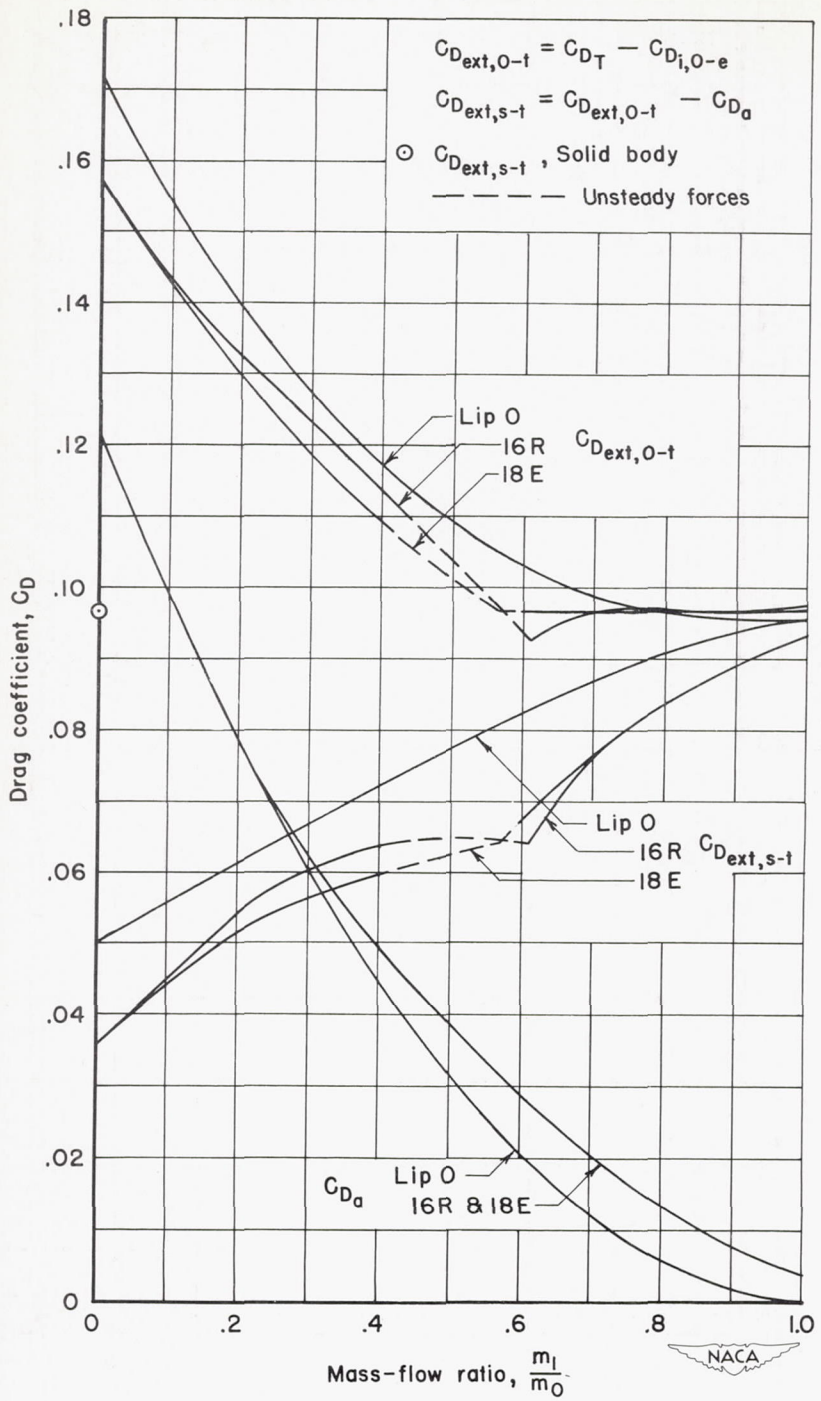

(a) $M_0 = 0.237$

Figure 19.- Variation of external- and additive-drag coefficients with mass-flow ratio for lips 0, 16R, and 18E.

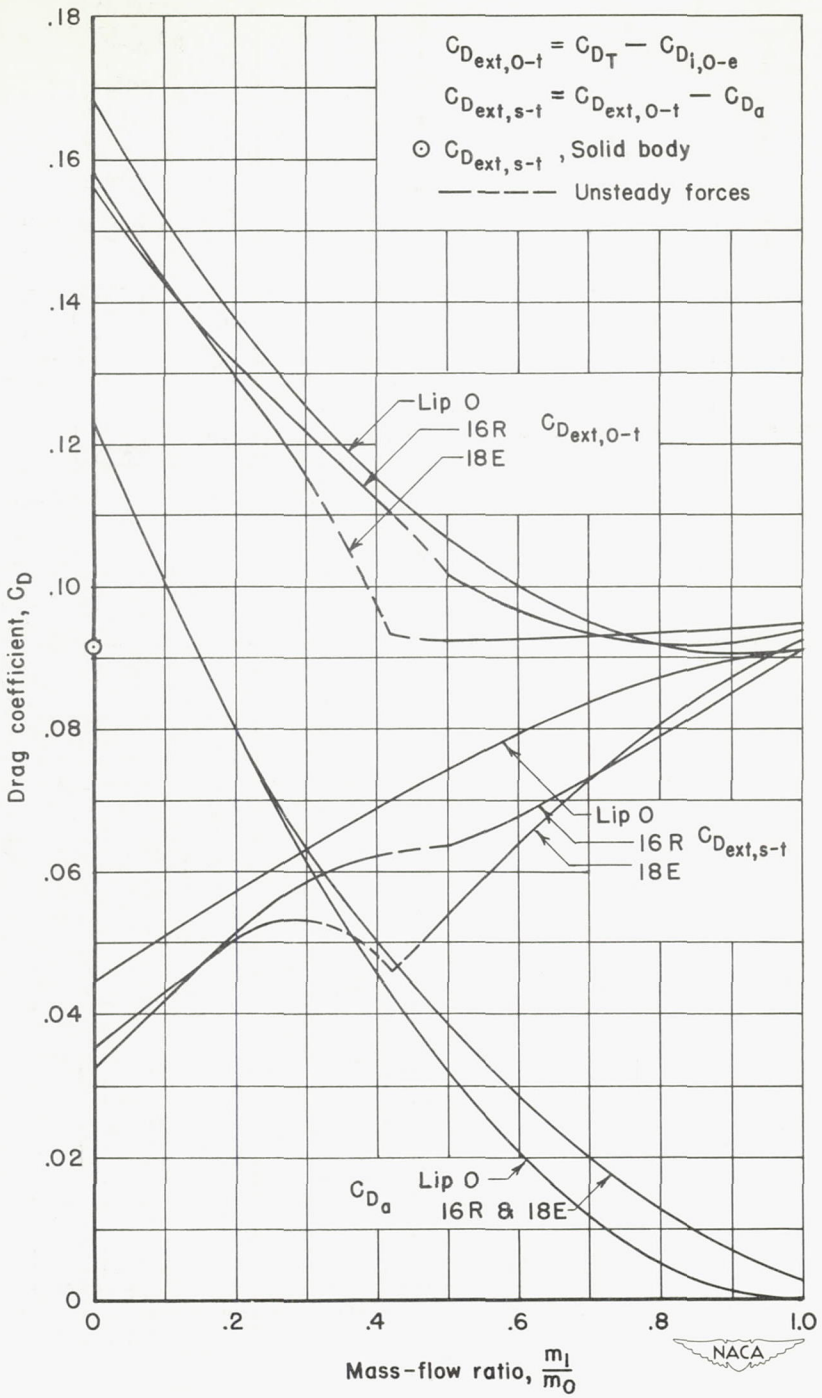

(b) $M_O = 0.330$

Figure 19.- Concluded.

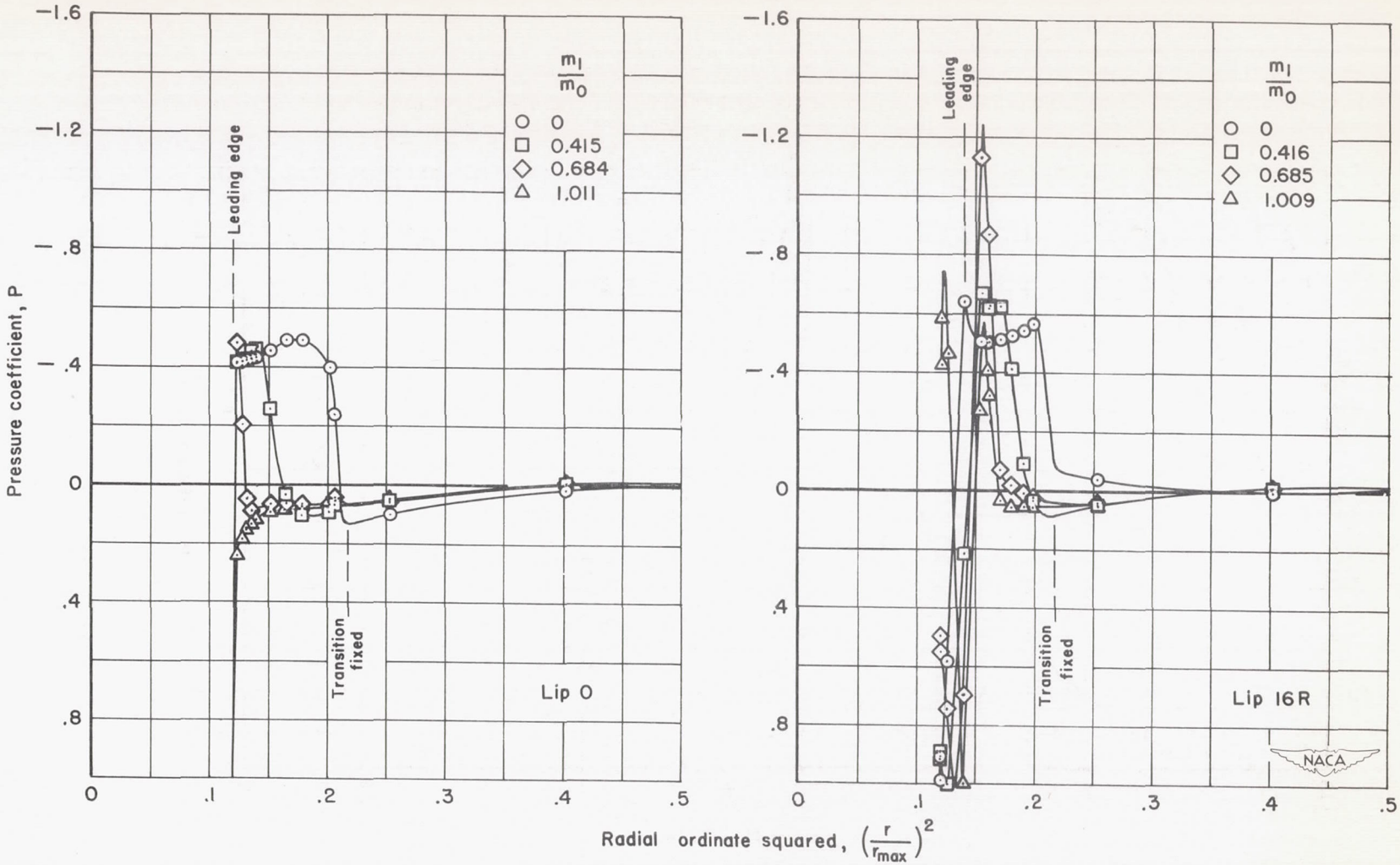

Figure 20.- Examples of pressure-coefficient variations over the forward portion of the model with lips 0 and 16R; $M_0 = 0.237$.

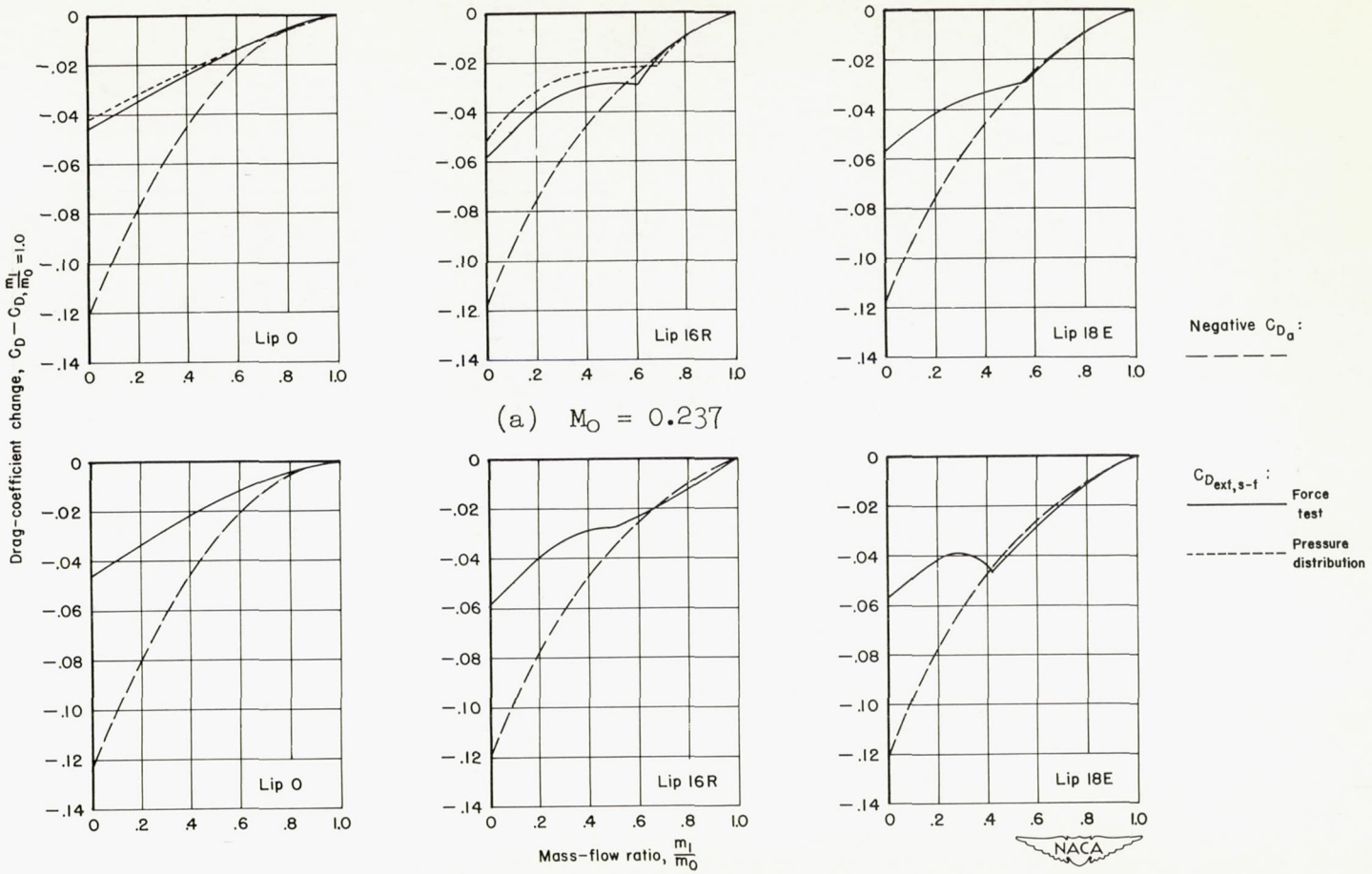

Figure 21.- Comparison of the variations of additive-drag and external-body-drag coefficients with mass-flow ratio for lips 0, 16R, and 18E.